JGR Solid Earth

RESEARCH ARTICLE
10.1029/2021JB023891

Formation of the Igneous Logi Ridge, NE Atlantic

Pingchuan Tan[1,2] and Asbjørn Johan Breivik[3]

[1]Key Laboratory of Submarine Geosciences, Ministry of Natural Resources & Second Institute of Oceanography, Ministry of Natural Resources, Hangzhou, China, [2]Southern Marine Science and Engineering Guangdong Laboratory, Zhuhai, China, [3]Department of Geosciences, Centre for Earth Evolution and Dynamics, University of Oslo, Oslo, Norway

Key Points:

- We represent a high-resolution 3D volume model of the Logi Ridge from refraction/reflection seismic data, bathymetry, and gravity
- Estimates of the elastic plate thickness under the Logi Ridge show a short main igneous phase with a magma production rate of 0.07–0.15 m^3/s
- The Logi Ridge is not caused by high mantle temperature but in part by the enriched mantle presently seen at the Eggvin Bank to the south

Correspondence to:
P. Tan,
tanpc@sio.org.cn

Citation:
Tan, P., & Breivik, A. J. (2022). Formation of the igneous Logi Ridge, NE Atlantic. *Journal of Geophysical Research: Solid Earth*, *127*, e2021JB023891. https://doi.org/10.1029/2021JB023891

Received 23 DEC 2021
Accepted 2 MAR 2022

Abstract The igneous Logi Ridge is located in the NE Atlantic north of the West Jan Mayen Fracture Zone on oceanic crust. The origin of the ridge may relate to the increased influence of the Iceland plume in the Oligocene though the exact mechanism is uncertain. We estimate the igneous volume and magma production rate of the ridge from 10 transects, comprising a refraction profile, six reflection profiles, and three bathymetric profiles. The refraction profile shows up to 12 km crustal thickness of the ridge, and the forward gravity modeling and/or isostatic balancing shows that this is characteristic for most of the ridges. A 3D volume model was created by interpolating between profiles and subtracted the similarly made regional crustal thickness (5–7 km), which gives an excess magma volume of $(1.7 \pm 0.6) \times 10^{13}$ m^3. The admittance function between bathymetry and gravity indicates an elastic plate thickness of 3–5 km during the main ridge formation. This is consistent with the ridge being built on oceanic crust from Oligocene to earliest Miocene, indicating a main magmatic phase of ~5 Ma duration, which gives a magma production rate of 0.07–0.15 m^3/s, comparable to the Louisville Seamount Chain (LSC). However, the lower crustal velocities of the refraction profile differ from that of the Louisville Guyot in the LSC, suggesting that the melting event was not mainly caused by high mantle temperature, instead it may have been caused in part by the enriched mantle presently seen at the northern end of the Kolbeinsey Ridge to the south.

Plain Language Summary The igneous Logi Ridge is located in the North Atlantic Ocean, near the Norwegian Jan Mayen Island. The origin of the Logi Ridge may relate to the increased influence of the Iceland plume in the NE Atlantic in the Oligocene though the exact mechanism is uncertain. We use density modeling calibrated to one refraction profile to develop the methodology, which was applied to six reflection profiles and three bathymetric profiles to estimate the igneous volume of the ridge. Estimates of the elastic plate thickness at the time of ridge loading constrain the time of formation well and indicate a short main igneous phase, mainly Oligocene. The magma production rate is estimated to be 0.07–0.15 m^3/s, which is comparable to the plume-induced Louisville Seamount Chain (LSC) in the Pacific, similarly formed on young oceanic lithosphere. The lower crustal velocity of the Louisville Guyot in the LSC, which is a seamount of similar dimensions, is consistent with a hot plume origin. However, velocity is significantly lower for the Logi Ridge, suggesting that the formation was not driven by the significantly elevated temperature. The enriched mantle component currently sourcing magmatism at the northern segment of the Kolbeinsey spreading ridge to the south could have contributed.

1. Introduction

The NE Atlantic developed in two major tectonic events, both affected by the Iceland plume. During the Paleocene-Early Eocene breakup between Greenland and Europe, the formation of the continental margins was accompanied by massive magmatism, forming the major part of the Northeast Atlantic Igneous Province (NAIP). These margins are characterized by thick, high-velocity lower crustal layers (HVLC) and Seaward Dipping Reflectors (SDRs) (e.g., Abdelmalak et al., 2016; Breivik et al., 2014; Geissler et al., 2017; Holbrook et al., 2001; Voss & Jokat, 2007; Voss et al., 2009). During the Oligocene to Early Miocene, the influence of the Iceland Plume increased in the NE Atlantic (e.g., Mjelde et al., 2008). As a direct consequence of this, the Jan Mayen micro-continent (JMMC) was rifted off East Greenland by the spreading axis jump from the Aegir Ridge to the Kolbeinsey Ridge (e.g., Mjelde et al., 2008; Nunns, 1982) (Figure 1). Lava flows along the western margin of the JMMC (Blischke et al., 2017, 2019) and Oligocene volcanism in East Greenland, including Traill Ø Island landward of the West Jan Mayen Fracture Zone (WJMFZ) (Franke et al., 2019; Price et al., 1997) show that the rifting of the JMMC off East Greenland was in some parts associated with substantial magmatism. Also the

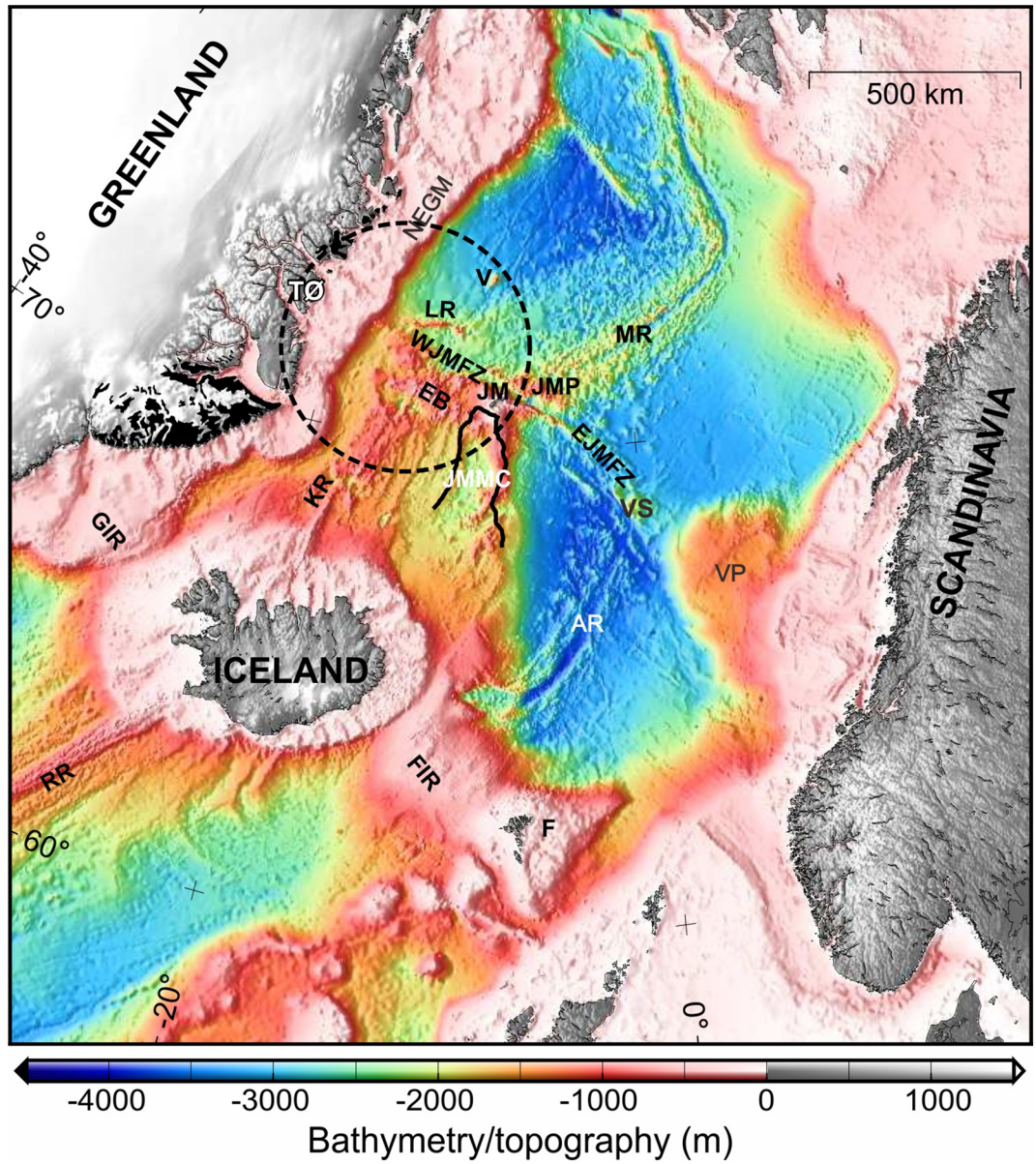

Figure 1. Regional elevation map (ETOPO 2V2) (National Geophysical Data Center, 2006), where the study area is indicated by the dashed circle (Figure 2). Black areas onshore Greenland indicate Early Cenozoic basalt flows or intrusions (Noble et al., 1988). The black solid line represents the Continental Ocean Boundary around the JMMC by Blischke et al. (2017). AR: Aegir Ridge, EB: Eggvin Bank, EJMFZ: East Jan Mayen Fracture Zone, F: Faeroes, FIR: Faeroes-Iceland Ridge, GIR: Greenland-Iceland Ridge, JM: Jan Mayen, JMMC: Jan Mayen microcontinent, JMP: Jan Mayen Plateau, KR: Kolbeinsey Ridge, LR: Logi Ridge, MR: Mohn's Ridge, RR: Reykjanes Ridge, NEGM: NE Greenland Margin, TØ: Traill Ø, V: Vesteris Seamount, VP: Vøring Plateau, VS: Vøring Spur, WJMFZ: West Jan Mayen Fracture Zone.

oceanic crust formed at the Middle Kolbeinsey Ridge since the Late Oliocene breakup has a greater than normal crustal thickness at 9 km (Kodaira et al., 1998a). However, the lack of SDRs and HVLC along the western margin of the JMMC (Kodaira et al., 1998a) and only a minor HVLC at the conjugate East Greenland margin (Hermann & Jokat, 2016) show that this later stage breakup magmatism was substantially smaller than the Early Eocene magmatism. In order to understand this second event, we need better quantification of the associated magmatism in the area. The formation age of the Logi Ridge north of the WJMFZ was determined from reflection seismic to be mainly Late Oligocene to Early Miocene (Tan et al., 2019). Similarly, Franke et al. (2019) indicate a Late Oligocene age for the magmatism landward of the ridge on the East Greenland shelf, also from reflection seismic

data, relating it to the rifting off of the JMMC. While the development of the Logi Ridge is reasonably well constrained (Tan et al., 2019), the magmatic event itself needs to be quantified in terms of volume and magma production rate. Magmatic volume calculations for the East Greenland margin are presented by Voss et al. (2009), but to our knowledge, this is currently lacking for magmatic structures in the area between the SE Greenland margin to and including the island of Jan Mayen.

A regional 3D gravity model of the Jan Mayen-East Greenland region with a horizontal node spacing of 10 × 10 km was published by Tan et al. (2018). The calculated gravity response over the Logi Ridge from that model is up to 50 mGal higher than observed, showing that the crustal density model of the Logi Ridge needs to be improved. In order to build a more precise crustal model, we use the only published seismic refraction profile (AWI20030500) that crosses the Logi Ridge (Voss & Jokat, 2007) that was also used for the regional model of Tan et al. (2018), but further include the seismic reflection lines of Tan et al. (2019). These profiles also have recorded ship-track gravity, and density models of the profiles can be tested by gravity modeling. From the refraction profile, we developed a simplified modeling procedure that can also be used with the limited boundary conditions provided by the reflection seismic lines. Satellite gravity has a resolution limit of just below 30 km wavelength (Gaina et al., 2011) and does not measure the narrow ridge well, typically showing 20–30 mGal too low gravity above the peak of the ridge. Four additional profiles, one reflection seismic line from Tan et al. (2019) and three bathymetric profiles were added to obtain a complete coverage of the ridge. These do not have ship-track gravity, but isostatic balancing was used to estimate crustal structure, combined with constraints by the ties with the refraction profile. The resulting crustal structure along the profiles is then used to build a high-resolution (2 × 2 km horizontal node spacing) crustal volume model of the ridge area.

Also the elastic thickness of the lithosphere at the time of ridge loading is estimated. When compared to models of the temperature development of the lithosphere, further constraints on the main ridge building time can be obtained. From the magmatic duration and volume estimates, the magma production rate can be estimated, enabling comparison to other events. Finally, the velocity structure of the ridge from the refraction profile is compared to the results from other seamounts formed at different conditions to further constrain the mechanism behind the magmatic event.

2. Geological Background

The breakup between Greenland and Europe established three spreading axes in the Early Eocene; the Reykjanes Ridge to the south, the Aegir Ridge in the middle, and the Mohn's Ridge to the north (Figure 1). The corresponding margin segments were to various degrees influenced by the Iceland Plume (e.g., Holbrook et al., 2001; White et al., 2008), resulting in volcanic margin formation (Breivik et al., 2009, 2014; Voss & Jokat, 2007). The Aegir and Mohn's ridges were separated by the East Jan Mayen Fracture Zone (EJMFZ), and the initial breakup occurred along the eastern JMMC, producing a volcanic margin similar to the conjugate Møre-Faroes margin (Breivik et al., 2006, 2012; White et al., 2008). Rifting of the JMMC from East Greenland commenced in the Early Oligocene and gradually propagated northward (Blischke et al., 2017). During the early Miocene, the breakup between the JMMC and Greenland was completed (Blischke et al., 2017) by establishing the Kolbeinsey seafloor spreading ridge, connected to the Mohn's Ridge via the newly formed WJMFZ (Figure 1).

2.1. JMMC Breakup-Related Magmatism

The western margin of the JMMC lacks a HVLC and has a very thin continental crust (~5 km) at the Jan Mayen Basin, created by a prolonged extensional phase prior to the Kolbeinsey Ridge formation (Kodaira et al., 1998a, 1998b; Mjelde et al., 2008). Based on a dense coverage of seismic reflection profiles, Blischke et al. (2019) established a Cenozoic seismic-stratigraphic framework for the western margin of the JMMC. Their results show widespread shallow marine volcanic flows and intrusive sills that were emplaced during the Oligocene. On the conjugate East Greenland margin, Hermann and Jokat (2016) observed a 3-km-thick high-velocity lower crust beneath the continent-ocean transition zone on seismic refraction profiles just south of the WJMFZ. They suggested that the high-velocity lower crust is due to excess magmatism tied to the WJMFZ formation during the continental breakup of the JMMC off East Greenland. A large elongated magnetic high (Traill Ø Igneous Complex (TIC)) is observed on the shelf landward of the western end of the WJMFZ (Figure 2). Traill Ø is located at the westernmost end of the TIC (Figure 2), where syenitic intrusions exposed onshore are dated to

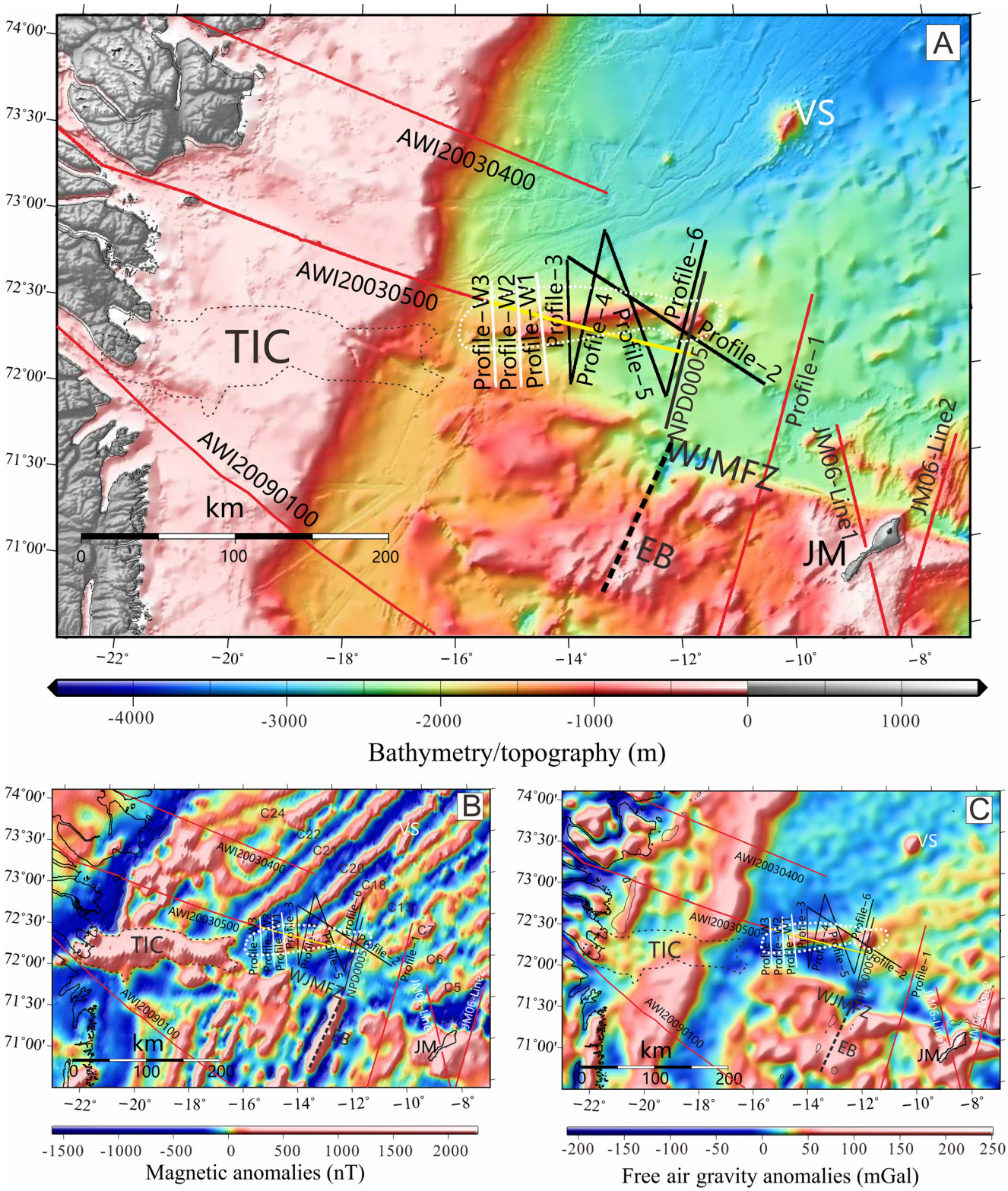

Figure 2.

34–36 Ma, coeval with the rifting of the JMMC (Noble et al., 1988; Price et al., 1997) (Figure 1). Tan et al. (2019) found that the onset of formation of the Logi Ridge also started in the Oligocene, and that its formation correlates with a regional dynamic topography rise expected to come from the increasing Iceland Plume influence in the asthenosphere.

2.2. Post JMMC Breakup Magmatism of the Area

After the JMMC breakup, there was extensive post-breakup magmatic activity in our study area besides that of the Logi Ridge. The island of Jan Mayen is of igneous origin and has an active volcano. A seismic refraction study shows an igneous crustal thickness of 25 km beneath the island (Kandilarov et al., 2012). The magmatism is derived from deep, low-degree mantle melting (Trønnes et al., 1999). Adjacent to the island, excess magmatism is observed across the WJMFZ at the southern tip of the Mohn's Ridge, where the oceanic crust is up to 12-km thick (Kandilarov et al., 2012). The geochemical composition is similar to that of the Jan Mayen magmatism (Elkins et al., 2016; Mertz et al., 2004). Between Jan Mayen and Greenland, the Eggvin Bank is a shallow area with magma-rich spreading at the northern segment of the Kolbeinsey Ridge. It is confined to the south by a small offset on the spreading ridge and to the north by the WJMFZ (Figure 2). The bank has been dredged both on-axis and off-axis (e.g., Elkins et al., 2011, 2016; Haase et al., 2003), showing enriched isotope signatures indicating an eclogite-rich source, distinct from adjacent segments of the spreading ridge system. The crustal structure of the eastern Eggvin Bank was established by a refraction seismic study, showing igneous crust with a thickness of 8–13 km (Tan et al., 2017). The greatest thickness is underneath two large seamounts. Also the area north of the Logi Ridge is active with recent magmatism on the Vesteris Seamount. Dredged samples indicate that the magmatism is derived from a depleted mantle source of non-plume origin (Haase & Devey, 1994). There is also minor recent magmatic growth and tectonic activity southeast of the Logi Ridge, which correlate with prolonged dynamic uplift there (Tan et al., 2019). Several papers argue for a separate Jan Mayen mantle plume (e.g., Elkins et al., 2016; Rickers et al., 2013; Schilling, 1999). On the other hand, Tan et al. (2018) found that the Jan Mayen magmatism is most likely a result of the shallow part of the asthenospheric flow out from the Iceland Plume in the south, which is being diverted to the east by the WJMFZ due to the associated lithospheric thickness increase to the north of the Kolbeinsey Ridge. It is, however, possible that the deeper part of this flow is not diverted and responsible for some of the magmatism seen north of the Kolbeinsey Ridge.

3. Data and Methods

3.1. Data

The data used for this study come from four different sources. The Alfred Wegener Institute (AWI) supplied the 2D crustal velocity model AWI20030500, including free-air ship-track gravity measurements (Voss & Jokat, 2007). The biggest data set consists of five single-channel seismic reflection lines (Profiles 2–6) that were collected by the University of Bergen and Oslo, including ship-track free-air gravity and echo-sounder recordings (Tan et al., 2019). In addition, we use one multichannel seismic reflection line (NPD0005) supplied by the Norwegian Petroleum Directorate that covers the eastern Logi Ridge (Figure 2) (Tan et al., 2019). Since the western part of the ridge is not covered by seismic data, we use the IBCAO v.4 bathymetry compilation (Jakobsson et al., 2020) to extract three additional bathymetric profiles for the modeling. The basement depths of these three profiles are derived from the regional sedimentary model of Tan et al. (2018).

3.2. Methods

3.2.1. Density Modeling

For calculating the forward gravity response of the density models, we use an in-house (University of Oslo, unpublished)-developed program based on the 2D algorithm by Talwani et al. (1959). The start and end of the

Figure 2. Location of seismic data in the study area shown on IBCAO v.4 bathymetry map (Jakobsson et al., 2020) (a), magnetic map (Verhoef et al., 1996) (b), and satellite free-air gravity map (Gaina et al., 2011) (c). The seismic reflection lines used in this study are shown as black solid lines, three bathymetry profiles as white solid lines, and published seismic refraction lines (Hermann & Jokat, 2016; Kandilarov et al., 2012; Tan et al., 2017; Voss & Jokat, 2007) as red solid lines with the part used in this study marked by the yellow solid line. The area of the Traill Ø igneous complex and Logi Ridge is indicated by thin dotted black and white lines, respectively. The Northern Kolbeinsey spreading ridge is shown by a thick black-dashed line. Seafloor spreading anomalies annotations are from Gaina et al. (2017). EB: Eggvin Bank, JM: Jan Mayen, TIC: Traill Ø Igneous Complex, WJMFZ: West Jan Mayen Fracture Zone, VS:Vesteris Seamount.

profiles have been extended by 1,000 km in order to avoid edge effects during the gravity modeling. Forward gravity modeling over oceanic lithosphere of varying age must also include the temperature-induced density differences in the mantle. We use a forward 2D finite element temperature modeling algorithm to simulate the temperature development based on the oceanic age along all transects (Lee et al., 1980). See Breivik et al. (1999) for a description of parameters and procedure. Seafloor ages are derived from Gaina et al. (2017). Mantle density is estimated using the approach of Bai et al. (2014), which is based on both temperature and pressure.

Densities for the AWI20030500 crustal velocity model are derived using the Rayinvr internal conversion (Zelt & Smith, 1992). Constant density polygons then correspond to the average velocity of the velocity-determining polygons within the Rayinvr model. From that, a simplified gravity modeling procedure is developed that will reproduce a good gravity fit using the known crustal thickness combined with the estimated mantle densities to be applied to the other profiles.

Basement depth for the reflection seismic profiles was obtained from two-way time depth converted using the regional empirical velocity-depth trend for the sediments (V_p = 1.8 + 0.7Z km/s, Z: Sediment thickness in km) from Tan et al. (2019). The density-depth relationship of sediments in the Norwegian-Greenland Sea has been estimated by Engen et al. (2006) (ρ(Z) = 2890−990exp (−0.15Z) kg/m^3, where Z is depth from the seafloor in km). We divide the sedimentary package into ∼500-m-thick layers with constant densities. For each profile, the Moho depth is estimated, so that (a) there is a good fit between the calculated and ship-track gravity anomalies over the ridge and (b) a good fit at the tie to the AWI20030500 profile. For the profiles without ship-track gravity, we estimate the Moho depth underneath the ridge by the degree of local compensation of the ridge itself, compared to nearby profiles, and by ties to the refraction profile. For comparison, a local isostatic Moho is calculated for all the density models, which includes a mantle density model down to 125 km depth.

3.2.2. Lithospheric Strength During Loading

The plate strength at the time of the ridge loading along profiles can be estimated by calculating the transfer function (admittance) between bathymetry and free-air gravity in the frequency domain, which can be compared to theoretical admittance functions for different elastic strengths of the lithosphere (Watts, 1978). The method will give an equivalent thickness T_e of an elastic plate. The T_e of young oceanic lithosphere incorporates both parts of the crust and the upper mantle and correlates with the depth of the 450 ± 150°C contour (Watts, 1978). The results can therefore be compared to thermal models of the lithosphere at the ridge for given times to further constrain the time of the main ridge building. To dampen noise from profile ends, we uplift the bathymetry by 2,400 m and linearly taper each end of the profiles to zero over 100 km.

3.2.3. Igneous Process

In order to calculate the igneous volume of the ridge, we need both a volume model of the ridge as well as an estimate of the crustal volume before the emplacement of the ridge. The crustal volume of the ridge is estimated by interpolating the modeled profiles using GMT (Wessel & Smith, 1991). The crustal volume before the ridge emplacement can be estimated by interpolating the basement and Moho depths north and south of the ridge across the ridge area. These can similarly be interpolated into a 3D regional volume model that estimates the crustal thickness as it was before the ridge development. The excess magmatic volume of the ridge can then be estimated by subtracting the regional model from the ridge volume model. In order to calculate the magma production rate, we need to estimate the duration of magmatism. Tan et al. (2019) constrained the ridge development to be from the Oligocene until mid-Miocene. However, the main loading phase can be further constrained by the lithospheric flexural response to the ridge loading estimated here.

The temperature dependence of the mantle melting can be estimated by the correlation between the lower crustal seismic velocity (Vp) and total igneous crustal thickness (H) (e.g., Holbrook et al., 2001; Sallarès & Calahorrano, 2007). In situ lower crustal velocities are corrected for temperature and pressure following Holbrook et al. (2001). The pressure is calculated from the density model for all depths, and the pressure correction is 0.00022 km/s/MPa. The temperature correction is −0.0005 km/s/°C, assuming a linear temperature gradient from 10°C at the seafloor to 750°C at 40 km depth. In order to remove the effect of crustal alteration and porosity, all crustal velocities lower than 6.85 km/s are set to 6.85 km/s. If the excess volcanism is caused by the elevated mantle temperature, there should be a positive H-Vp correlation, while excess magmatism caused by active mantle upwelling and/or an enriched mantle source is expected to give a low-to-negative H-Vp correlation (Holbrook et al., 2001).

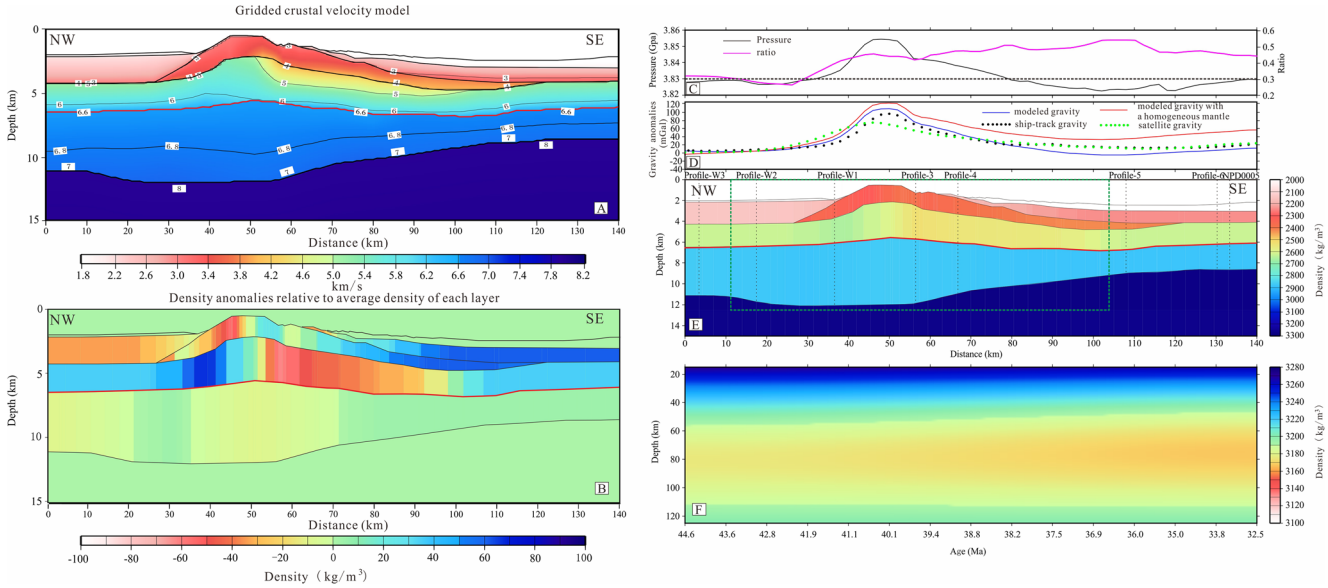

Figure 3. (a): Gridded crustal velocity model of the seismic refraction profile AWI20030500 (Voss & Jokat, 2007) (Figure 2). V_p velocities are annotated by small numbers. (b): density variations relative to mean density of each layer. (c–f): Results of 2D gravity modeling along AWI20030500. (c): The pressure at the bottom of the model at 125 km depth and the upper crustal thickness/total crustal thickness ratio along profile. (d): 2D gravity modeling showing calculated (blue line) and observed ship-track gravity (black dots) and satellite gravity (green dots) (Gaina et al., 2011). (e): The crustal density model derived from the OBS model (Voss & Jokat, 2007). The red solid line along the profile represents the upper/lower crustal boundary. The dashed green box shows the area of the ridge (white-dashed line on Figure 13) used for magma volume calculation. Tie points between the lines are also indicated. (f): The mantle density estimated down to 125 km by forward temperature modeling based on the oceanic seafloor ages indicated at the bottom (Gaina et al., 2016).

4. Results

4.1. Initial Density Modeling of Profile AWI20030500

The seismic refraction profile has two sedimentary layers with a combined thickness of up to 2.0 km (Figure 3). The upper sedimentary layer consists of unconsolidated deep sea sediments with velocities of 1.6–2.4 km/s, which converts to densities of 1,600–1,800 kg/m^3. The lower layer has laterally variable seismic velocities of 2.4–3.1 km/s, which gives densities of 1,800–2,200 kg/m^3. The boundary between the upper and lower crust is defined by the 6.6 km/s contour and is fairly level at 6 km depth. The density of the upper and lower crust varies between 2,200 and 2,600 kg/m^3 and 2,870–2,900 kg/m^3, respectively. The upper 2 km of the ridge itself has crustal velocities somewhat lower than the upper oceanic crust adjacent to the ridge consistent with basaltic rocks with large porosity. The crustal thickness underneath the ridge crest is up to 12 km. To the NW side of the Logi Ridge, the oceanic crust is 7 km thick, while to the SE, it is 5 km thick, reflecting a general thinning away from the margin.

Figure 3b shows the density anomalies for each layer compared to its average density along profile. The lower sedimentary layer shows a general increase of up to 100 kg/m^3 from the northwest to the southeast. The uppermost layer of the ridge itself shows the same trend. The layer underneath, which is continuous with the upper oceanic crust to the side of the ridge, has the lowest densities in the southeast flank of the ridge with variation of up to 120 kg/m^3. The density of the lower crust shows little variation (±10 kg/m^3).

The pressure at the bottom of the model does not show any regional trend between the profile ends, indicating that the thermal-based mantle density model is reasonable. Outside of the Logi Ridge, the pressure is about 3.828 GPa, while under the ridge, it is 3.855 GPa. This implies that there is some regional compensation as would be expected if the ridge grew on oceanic lithosphere with some flexural strength. Over the crest of the Logi Ridge, the calculated gravity is about 10 mGal higher than observed. This may be due to inaccuracy in determining the upper crust velocity/density under the ridge crest. The calculated gravity is also somewhat higher on the northern flank of the ridge (Figure 3d). This part shows increased velocities in the upper crust, resulting in a corresponding density contrast (Figure 3b), which may have been overestimated, if crack porosity is the main cause of the velocity variations. The density model also gives ~20 mGal lower value than that observed to the

southeast of the Logi Ridge (Figure 3c). This corresponds to an area of slightly reduced pressure at the bottom of the model, indicating a mass deficit here. Since the profile is oblique to the ridge, 3D effects may also be a source to discrepancies at the flanks. Overall, the gravity model is reasonably consistent with the crustal structure of the seismic refraction profile.

4.2. Simplified 2D Density Model of Profile AWI20030500

A simplified modeling procedure for the AWI20030500 profile is developed following the procedure described in Section 3.2, where we determine the parameters that are to be used in the subsequent modeling. The sedimentary density model is derived from the density-depth relationship by Engen et al. (2006). The crustal density model is simplified into two layers. Since the upper part of the Logi Ridge has lower density compared to the upper oceanic crust surrounding it (Figure 3b), we tested densities from 2,250 to 2,550 kg/m^3 in 100 kg/m^3 steps for the upper layer. Figure 4 shows the results, where an upper crustal density of 2,350 kg/m^3 gives the best gravity fit, slightly better than the initial model. The density of the lower layer is kept at 2,900 kg/m^3, and the depth of the upper/lower crustal boundary is 6 km.

To estimate the uncertainty of the procedure, we first establish the extreme boundaries of the model. The isostatic Moho under the ridge is at a depth of up to 18 km, which is significantly deeper than that of the refraction profile. The peak gravity response from the isostatic model is also 40 mGal less than that observed (Figure 4b). For the regional crustal model, we estimate a Moho about 2 km shallower under the ridge than the refraction profile from which the corresponding gravity response becomes 10–15 mGal higher than that observed (Figure 4b). The regional Moho and the isostatic Moho represent the minimum and maximum Moho depth estimates under the ridge, respectively. However, changing the Moho depth under the central parts of the ridge by a maximum of ±1.7–1.8 km as shown in Figure 4c changes the gravity response by between 10 and 20 mGal over central parts of the ridge. Thus, the uncertainty of the Moho depth under the ridge crest that is obtained from the gravity modeling is estimated to be less than ±2 km (i.e., up to 2 km shallower or 2 km deeper) comparable to that of the seismic refraction line (Voss & Jokat, 2007). However, seismic and gravity uncertainties do not simply add up. The regional Moho limits the crustal thickness difference between the ridge and the surrounding oceanic crust since a positive crustal root is expected, so the minimum volume estimate is not affected. It is possible that the error upward could be slightly greater than the +2 km indicated here, but that is difficult to judge without a more targeted seismic error analysis for the ridge itself.

4.3. 2D Density Modeling of Additional Profiles

The results of the 2D density models are shown in Figures 5–10. They were generated following the method described in Section 3.2, and with parameters established in Section 4.2. The Moho geometry to the north and south side of the ridge is constrained by isostatic balancing, while under the ridge it is constrained by gravity modeling (Figure 2; Profiles 2–6) where possible. The Moho depth is also constrained by ties to the AWI20030500 profile (Figure 11). The ties to the refraction profile for Profile 3 and 4 are close to the center of the ridge. The gravity response support a 12 km Moho depth under Profile 3, while it indicates a slightly deeper Moho of 12.5 km for Profile 4. The other seismic profiles tie with the AWI20030500 profile off the ridge, except for Profile 2 which does not tie (Figure 2). Both Profile 5 and 6 give a good gravity fit with the Moho at 12 km depth. Profile NPD0005 runs close to Profile 6 and crosses the eastern seamount closer to its center. Since we do not have ship-track gravity here, we use the isostatic balancing as a guide and lift the Moho depth up to 12 km, the same depth as that of Profile 6. Profile 2 ties with four other profiles (Figures 2 and 5) and crosses the flanks of the eastern and western ridge segments. The results are consistent with the ties to Profiles 5 and 6 in predicting a maximum Moho depth of 10–11 km under the ridge flank.

The results from three additional transects in the west based on IBCAO V.4 bathymetry (Jakobsson et al., 2020) and the regional sediment thickness model from Tan et al. (2018) are shown in Figure 10. These profiles do not have high-resolution gravity to constrain them. However, Profile W-1 crosses the AWI20030500 Profile at the ridge flank (Figures 10 and 11), which gives a Moho depth of 12 km, about 1.5 km shallower than the isostatic Moho. From there, the depth is set to increase to 13 km under the summit of the ridge as seen on the nearby profiles (Figure 10). Profile W-2 ties the AWI20030500 profile off the ridge at a Moho depth of 11.5 km (Figure 11), which is consistent with the isostatic Moho there. The Moho under the ridge summit is

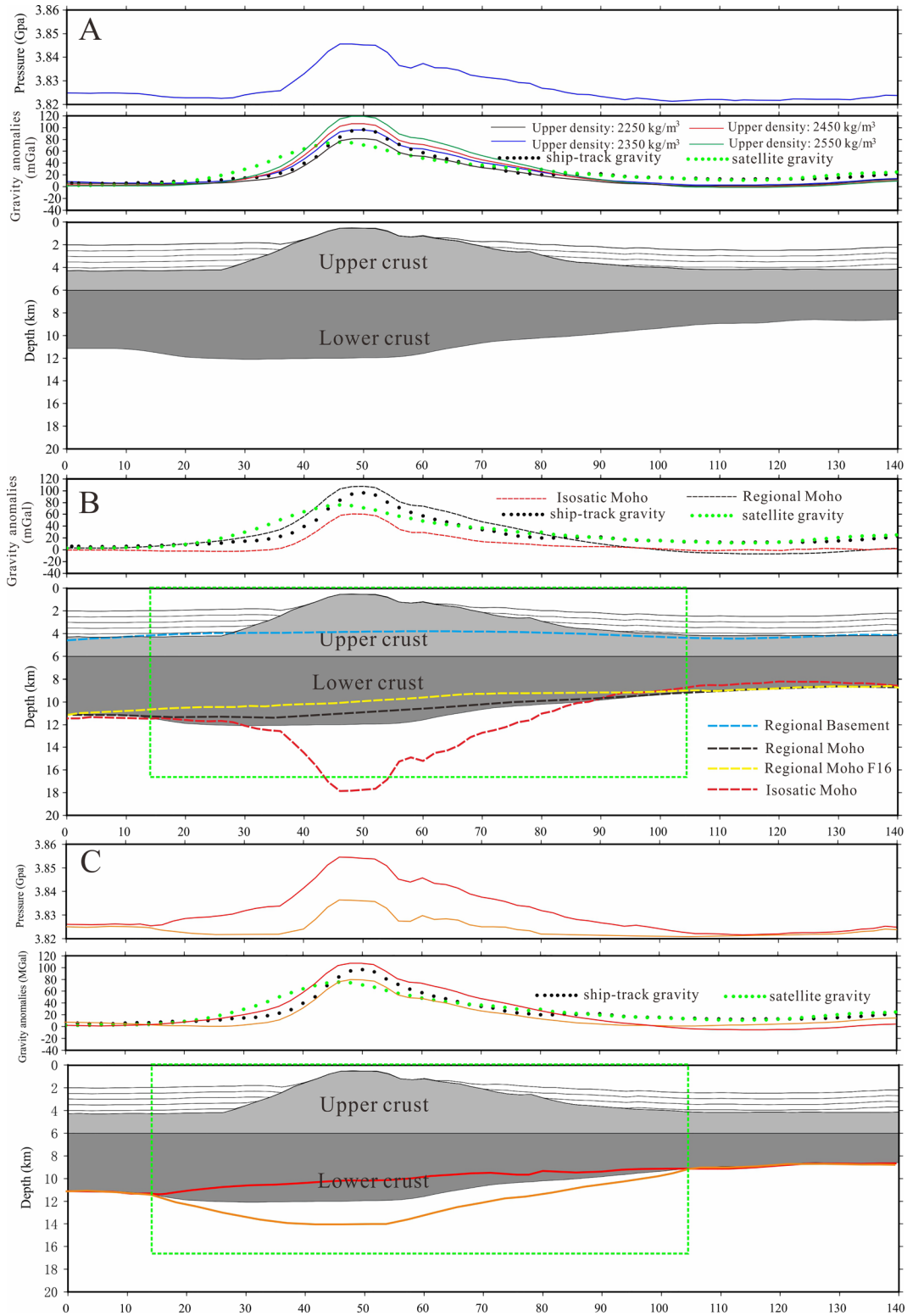

Figure 4. Estimation of modeling parameters, isostatic Moho, and regional basement/Moho. The crustal model of AWI20030500 (Voss & Jokat, 2007) is shown in gray. The mantle model is included, but not shown. Ship-track gravity is shown by black dots, while satellite gravity (Gaina et al., 2011) is shown by green dots. (a): Sensitivity test of upper crustal density (2,250–2,550 kg/m^3). (b): Our regional top basement and Moho are indicated by a dashed blue line and a dashed black line, respectively. The regional Moho from Funck et al. (2016) (regional Moho F16: dashed yellow line) is shown for comparison. The isostatic Moho is shown by the dashed red line. (c): Sensitivity test of the Moho depth of ±2 km under the summit. The green-dashed box indicates the area of the Logi Ridge used for ridge volume calculation.

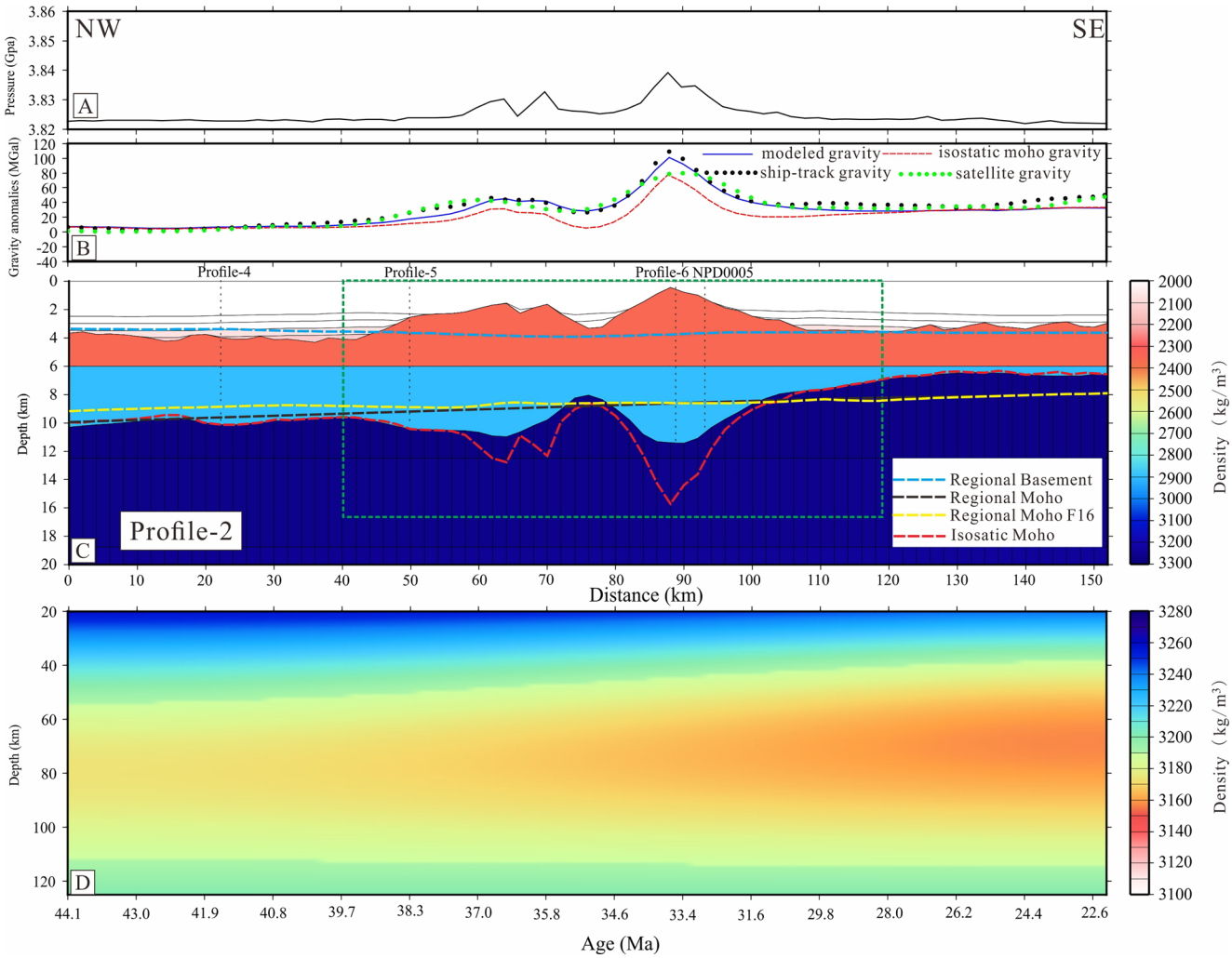

Figure 5. Results of 2D forward gravity modeling of Profile-2 (Figure 2). (a): Pressure at 125 km depth. (b): The gravity anomalies of the ship track (black dots), satellite (green) (Gaina et al., 2011), modeled (solid blue line), and modeled with isostatic Moho (dashed red line). (c): The crustal density model with ties to other lines is indicated. The green-dashed box shows area of the ridge (white-dashed lines on Figure 13) used for magma volume calculation. The dashed blue line is our regional basement, while the dashed black line is our regional Moho estimate, and the regional Moho from Funck et al. (2016) (regional Moho F16) is shown by dashed yellow line. (d): The mantle density estimated down to 125 km from forward temperature modeling using the oceanic seafloor ages (Gaina et al., 2016) indicated at the bottom.

taken to be about 2–2.5 km shallower than the isostatic Moho, and 13 km deep (Figure 10). Profile W-3 ties the AWI20030500 profile off the ridge, where the oceanic crust surrounding the ridge is thicker with a Moho depth of 11 km (Figures 10 and 11). In the final model, Moho is placed 1.5–2 km shallower than the isostatic Moho under the ridge summit, similarly at 13 km depth.

There is additional uncertainty due to the lack of high-resolution gravity constraints for these profiles. However, the thicker crust surrounding the western part of the ridge, combined with the reduced ridge relief, reduces the difference between the local isostatic Moho under the ridge to that of the surrounding Moho depth between a maximum of 3.5 and 4 km. Our preferred models reduce this difference to between 1.5 and 2.5 km. The Moho depth uncertainty should therefore be comparable to that of the eastern profiles. In general, the density models reproduce the gravity anomalies along the profiles reasonably well. The discrepancies are of a regional character, where there is a slight rise of the calculated gravity to the southeast (Figures 6 and 7). At the south end of Profile 6, the calculated gravity is about 20 mGal higher than that observed. The isostatic Moho is unusually shallow here and is extrapolated southward to avoid edge effects, which is probably not representative for the adjacent area and could contribute to the mismatch. Also along the southern part of Profile 2 and NPD0005, the crust is anomalously thin. Most likely, there are some deviations from the passive cooling model obtained from

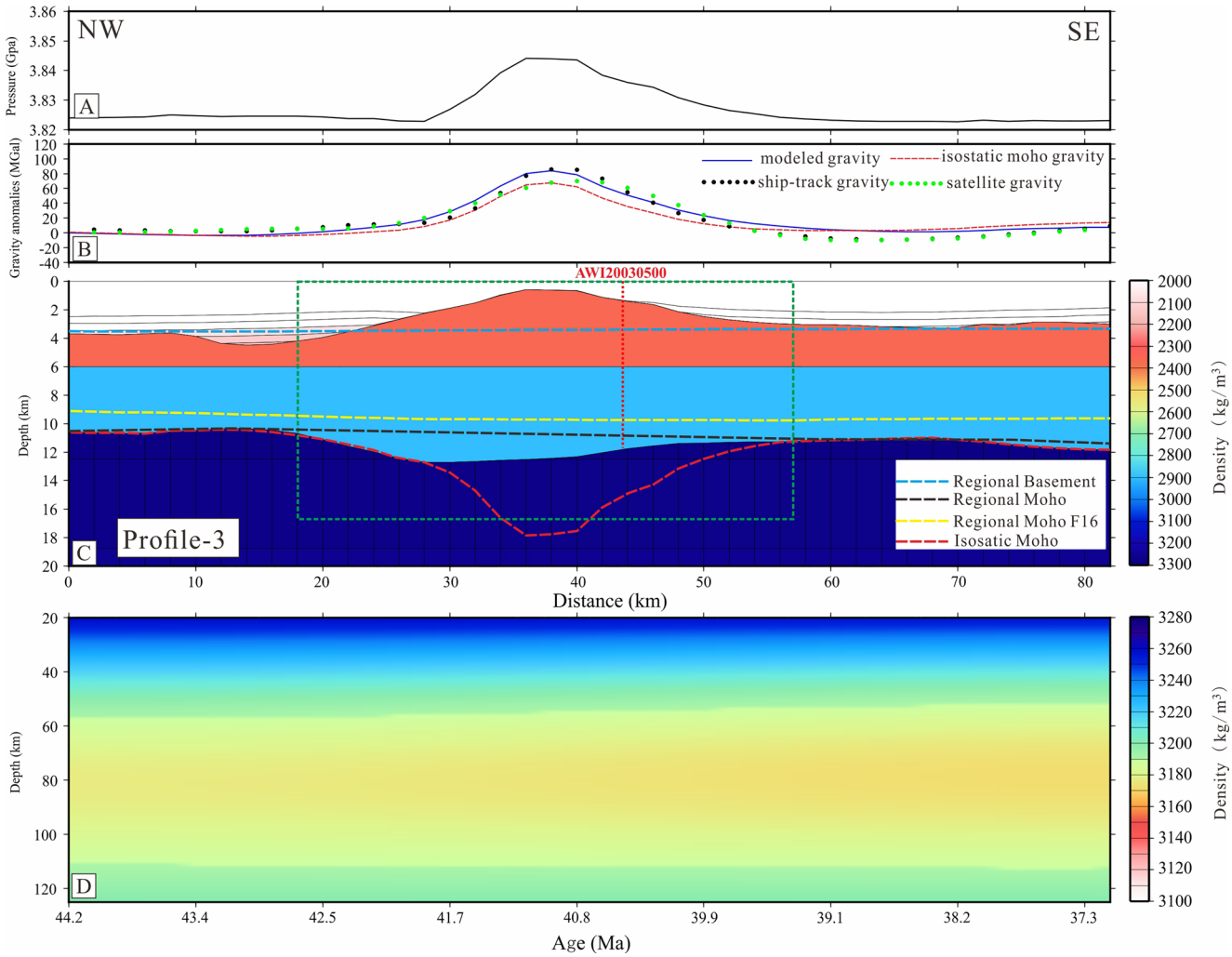

Figure 6. Results of 2D forward gravity modeling along Profile-3 (Figure 2). The tie to the AWI20030500 profile constrains the Moho depth near the summit of the ridge. Procedure and annotations are as in Figure 5.

our forward temperature modeling based on age only. However, this is a regional trend and should not affect the modeled ridge volume significantly.

4.4. Lithospheric Elastic Thickness During Ridge Emplacement

As seen from the isostatic balancing of the profiles, it is clear that there is some regional flexural support of the ridge topography. While the relationship between bathymetry and gravity can be used to estimate the lithospheric strength at the time of ridge emplacement, we need to estimate the longest, diagnostic wavelengths of the admittance function. Profile-2 and AWI20030500 offer the longest tracks and are therefore used for the analysis. The results of these two profiles are very similar, indicating that the elastic thickness of the oceanic lithosphere was between 3 and 5 km during the formation of the Logi Ridge (Figures 12a and 12b). In order to estimate the time of the main ridge building, we modeled the isotherm depths along Profile-2 and AWI20030500 for different times of the Logi Ridge development (Figures 12c and 12d). Profile 2 covers the eastern part of the ridge on the youngest seafloor, where the ridge is on 33–40 Ma old crust. Here, we calculate the thermal structure for 30, 25, and 15 Ma, the latter at the end of ridge development (Tan et al., 2019). Ridge emplacement must be later than 30 Ma, but well before 25 Ma. The AWI20030500 profile crosses middle to western parts of the ridge on crust 40–45 Ma old. Here, we calculate the thermal structure for 35, 25, and 15 Ma. The thermal structure of the lithosphere fits with a 35 Ma loading age, but not much younger. Thus, the timing of the main volume of the magmatism appears

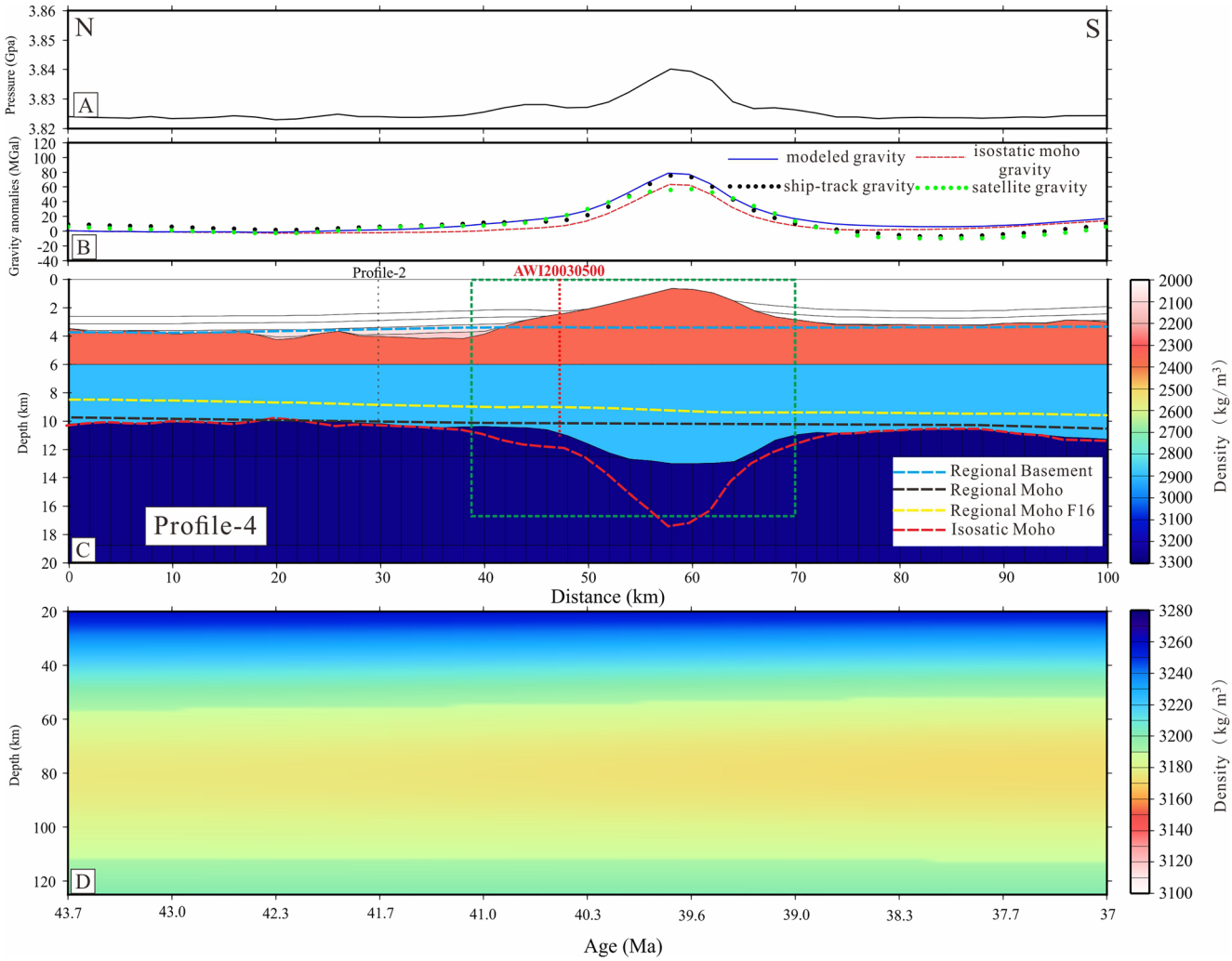

Figure 7. Results of 2D forward gravity modeling along Profile-4 (Figure 2). The AWI20030500 profile constrains the Moho depth under the flank of the ridge. Procedure and annotations are as in Figure 5.

to correlate with that of the Traill Ø magmatism observed onshore East Greenland at the time of incipient rifting off of the JMMC. However, the results also indicate that there may be some time transgression toward the east of the magmatism over a few million years (from early to late Oligocene).

4.5. Magmatic Volume and Emplacement Rates

The crustal structures from the modeled profiles were interpolated in GMT (Wessel & Smith, 1991) to create a 3D crustal model (comprising sedimentary and crustal layers). The model has a horizontal node spacing of 2 km in both northing and easting directions, which retains the main structural characteristics of the seismic profiles (Figures 13b and 13c). The regional Moho depth map similarly made from the models shows a gradually decreasing Moho depth from 13 km in the west to 7 km in the east, which reflects both the reduction of the crustal thickness with an increasing distance away from the volcanic margin as well as a younger oceanic lithosphere in the east (Figure 13a). The Moho depth under most parts of the Logi Ridge is 12–13 km as seen in the profile extracted along the ridge summit (Figure 13e). The intersection with our smoothed top regional basement map with the ridge is also shown in Figure 13e, which together with our regional Moho indicates the excess crustal thickness of the ridge.

Based on the bathymetric expression and seismic reflection profiles, we define an area around the region of the Logi Ridge (6.14×10^9 m^2) (white-dotted lines in Figure 13) within which we calculate the magmatic volume.

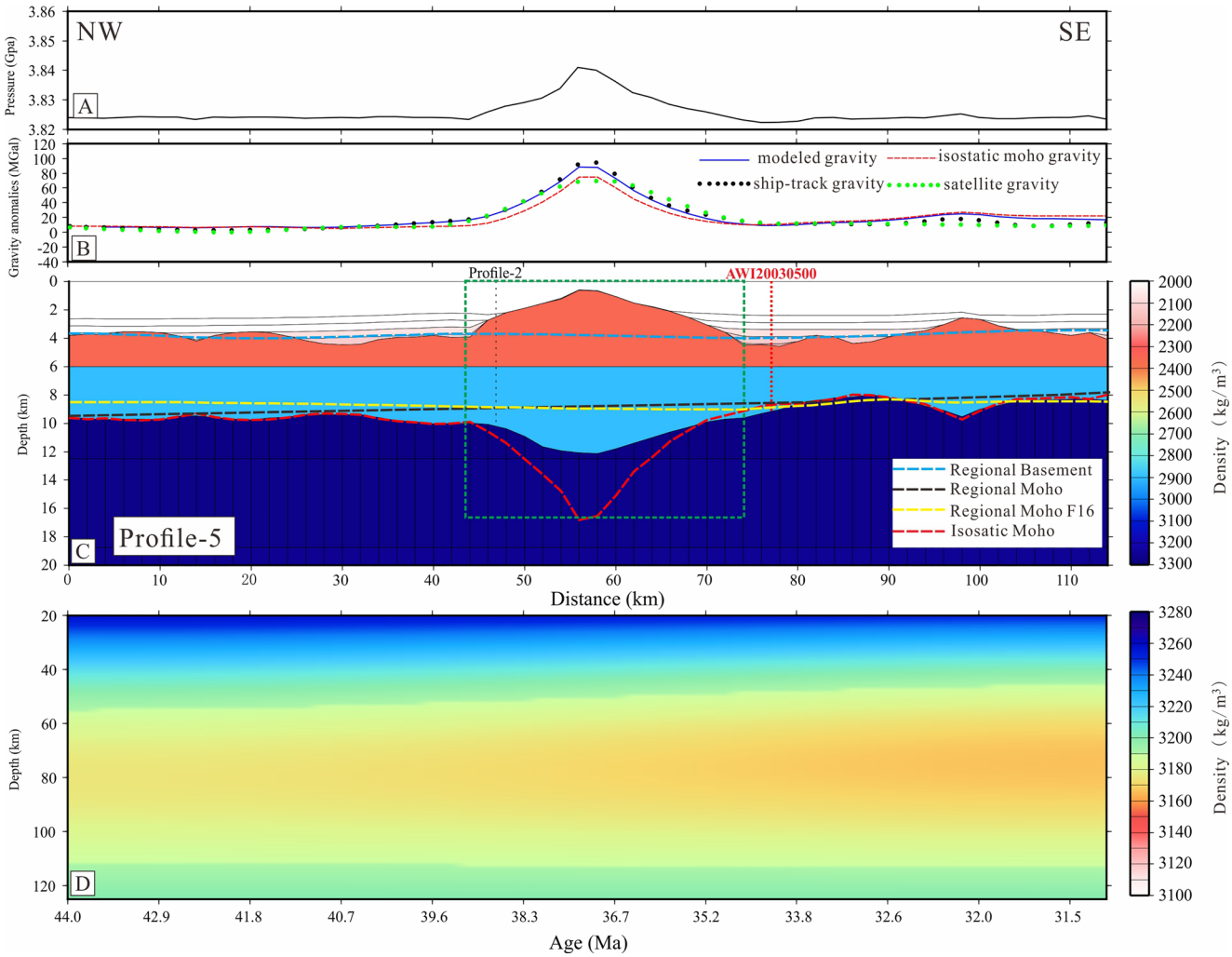

Figure 8. Results of 2D forward gravity modeling along Profile-5 (Figure 2). Procedure and annotations are as in Figure 5.

We do not consider any magmatic flows in the sedimentary layers, since they do not extend far away from the Logi Ridge, and the volume is small in comparison (Tan et al., 2019). The total volume of the igneous crust within this area is estimated to be 5.6×10^{13} m^3. The magmatic crustal volume before the Logi Ridge building is estimated from our regional model to be 3.9×10^{13} m^3 (Table 1). As seen in Figure 5, the regional crust becomes thicker than the modeled crust at the extreme southeastern end of the area. We do not allow negative volumes to be included in the volume calculation to correct for this. The estimated excess volume of the Logi Ridge is then 1.7×10^{13} m^3.

We compare our regional Moho to that of the regional Moho depth map of Funck et al. (2016), which is constrained by regional seismic refraction studies and gravity data with a long wavelength (Figure 13e). They are similar in the eastern part, but their model is slightly shallower in the west. Given the sparse seismic constraints, there may be a number of reasons for this as different principles were used for estimating Moho depth. Though it seems that our approach exaggerates the crustal thickness difference somewhat from west to east, possibly from deviations from a purely passive cooling model of the lithosphere, which in itself does not affect the estimated size of the crustal root underneath the ridge.

The gravity modeling reduces the estimated magma volume compared to a purely isostatic model. The modeling sensitivity indicates that the Moho depth under the peak of the ridge can be varied by less than ±2 km. But the Moho taper to the isostatic Moho is outside of the ridge, so an uncertainty of a ±1 km average for the whole region defining the ridge seems reasonable for the volume calculations. That gives a ridge volume uncertainty

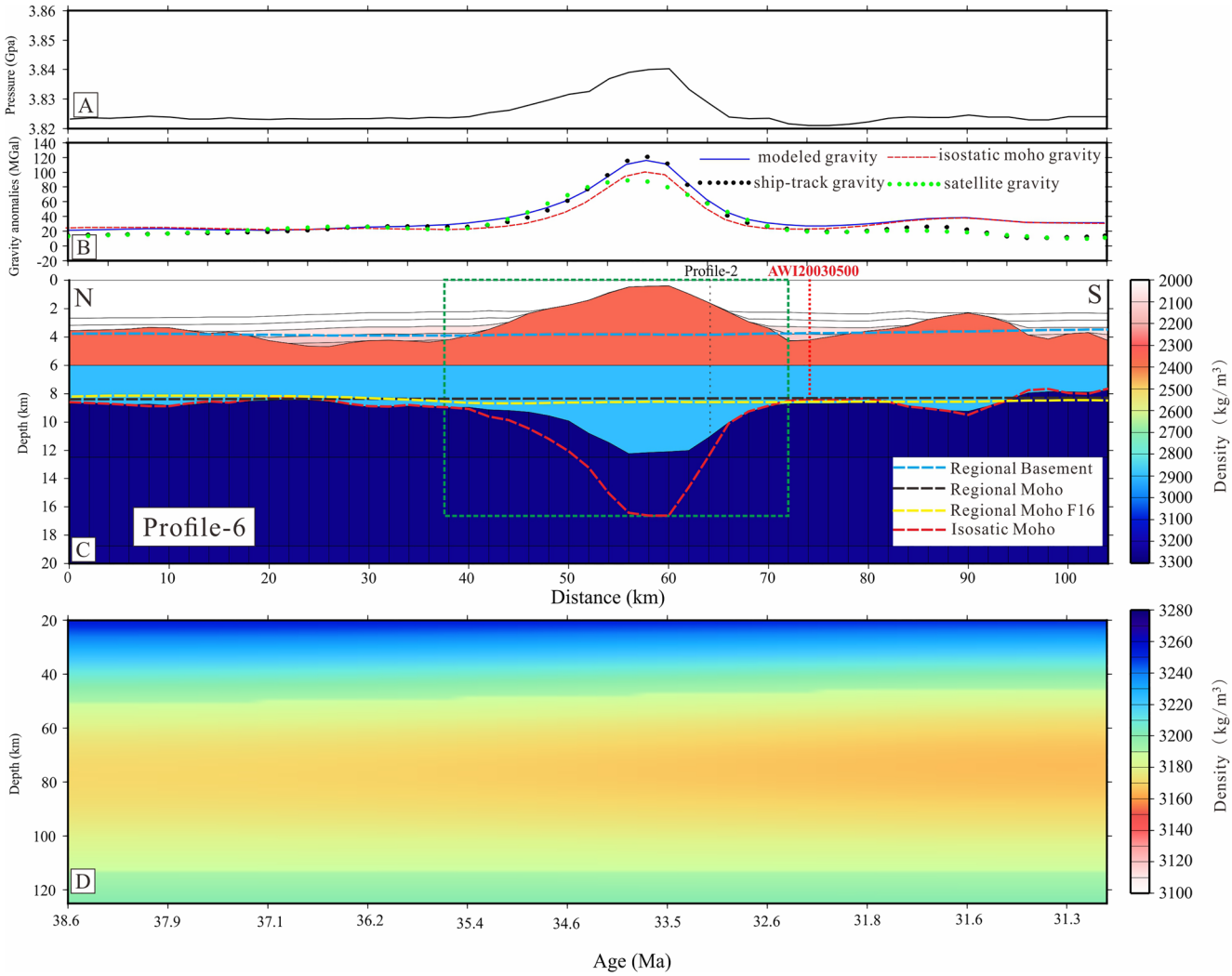

Figure 9. Results of 2D forward gravity modeling along Profile-6 (Figure 2). Procedure and annotations are as in Figure 5.

of $\pm 0.6 \times 10^{13}$ m^3 (Table 1), giving an excess volume of $(1.7 \pm 0.6) \times 10^{13} m^3$ (Table 1). The magma generation rate depends on the duration of the Logi Ridge formation. If building starts at the Eocene/Oligocene boundary at about 35 Ma and is over by the Middle Miocene at around 15 Ma (Tan et al., 2019), the maximum duration is 20 Ma. If the magma generation was evenly distributed over this time interval, then the generation rate becomes approximately 0.02–0.04 m^3/s. However, the magmatism is sparse in the latter stage of the ridge development (Tan et al., 2019), and the main loading appears to be of Oligocene age. If most of the magma were generated during the first 5 Ma, which seems probable, then that gives a magma generation rate of 0.07–0.15 m^3/s.

5. Discussion

The Logi Ridge is located along the same trend as the TIC on the shelf (Figure 2). The formation of the TIC has been related to the establishment of the WJMFZ during the rifting of the JMMC from Greenland around the Eocene/Oligocene boundary (e.g., Franke et al., 2019; Larsen et al., 2014; Price et al., 1997; Voss & Jokat, 2007), coeval with the start of the Logi Ridge formation (Tan et al., 2019). The results of our study also place the main magmatism to the time of the TIC formation, and a common cause seems likely. However, the Logi Ridge lies 100-km distant from the fracture zone and the WJMFZ formation itself does not seem to offer a suitable mechanism to explain either. The formation of the JMMC and the Logi Ridge occurs during the migration of the Iceland plume from underneath East Greenland to the continental margin (Mjelde et al., 2008), and excess magmatism of

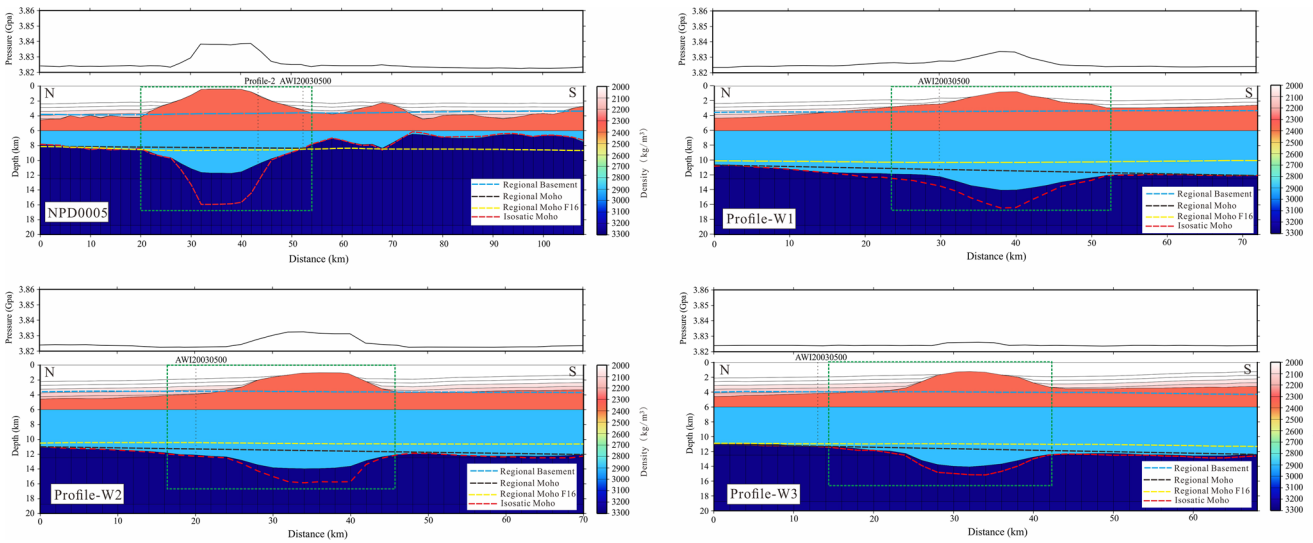

Figure 10. Results of isostatic modeling along NPD0005 in the east and the three bathymetric profiles in the west (Figure 2). Tie points between the lines are indicated on the crustal density models. Procedure and annotations are as in Figure 5. Moho depth is not be modeled here due to the lack of high-resolution gravity. Depth under the ridge is based on isostatic modeling and the ties to other profiles and by nearby results.

the Logi Ridge has been tied to this development (Tan et al., 2019). However, the exact mechanism is uncertain, and both an enriched mantle component seen at the northern segment of the Kolbeinsey Ridge (Eggvin Bank) (Elkins et al., 2011, 2016; Haase et al., 2003) as well as the elevated mantle temperature indicated by the dynamic topography (Rickers et al., 2013; Tan et al., 2019) could conceivably play a role in the Logi Ridge formation.

The crustal velocity structure of seamounts can be related to the melting process occurring in the mantle beneath them (Koppers & Watts, 2010). Various parameters can affect crustal velocity structure and sometimes result in a high-velocity lower crust under the seamount. Both mantle temperature and average melting depth are significant in that regard. Melting depth is related to the lithospheric plate thickness, which depends on age. For intraplate seamounts under a thick lithosphere affected by a hot plume, the average lower crustal velocity (>7.3 km/s) is higher compared to that of normal oceanic crust (7.0 km/s) (Sallarès & Calahorrano, 2007). However, hot spot-induced seamounts formed on or close to the ridge axis typically do not have such lower crustal high-velocity layers, since there is more shallow melting (e.g., Richards et al., 2013). For seamounts that do not originate from the elevated mantle temperature formed at the spreading axis, the excess magmatism is mainly accommodated by thickening of the lower crust; while if they are formed intraplate, the increased crustal thickness is achieved by thickening in both the upper and lower crust (Sallarès & Calahorrano, 2007) (Figure 14).

The crustal thickness under the Logi Ridge is up to 12 km on the AWI20030500 refraction profile (Voss & Jokat, 2007), and the ratio of upper crustal thickness versus total crustal thickness varies between 0.3 and 0.5 along profile (Figure 3) as the increased crustal thickness is achieved by thickening of both the upper and lower crust (Figure 14). The average lower crustal velocity (Figure 3a) is similar to that of normal oceanic crust (White et al., 1992), but significantly lower compared to intraplate eamounts affected by a hot plume (Sallarès & Calahorrano, 2007). In that regard, it falls well within what would be expected for seamounts formed off-axis, but on young oceanic lithosphere.

Compared to that of other magmatic events, the magma production rate estimated for the Logi Ridge is on the low end of the global data set (Mjelde et al., 2010). The higher production rate we estimate (0.07–0.15 m^3/s) seems to be the most realistic, but is still almost two orders of magnitude smaller than the present production at Hawaii (6 m^3/s) (Van Ark & Lin, 2004) and Iceland (8 m^3/s) (Mjelde & Faleide, 2009). It is, however, comparable to that of the Louisville hot spot (0.12 m^3/s) (Lonsdale, 1988). The magmatic production rate of the Louisville hot spot is calculated from the volume of structures above the surrounding seafloor (Lonsdale, 1988) and could be twice as high if roots were included (Contreras-Reyes et al., 2010), but still comparable. The Logi Ridge has a similar crustal thickness as that of the Louisville Guyot of the northern LSC surveyed by Contreras-Reyes et al. (2010) (12 vs. 13 km) (Figure 15). This is one of the larger seamounts of the LSC and is about twice as broad at the

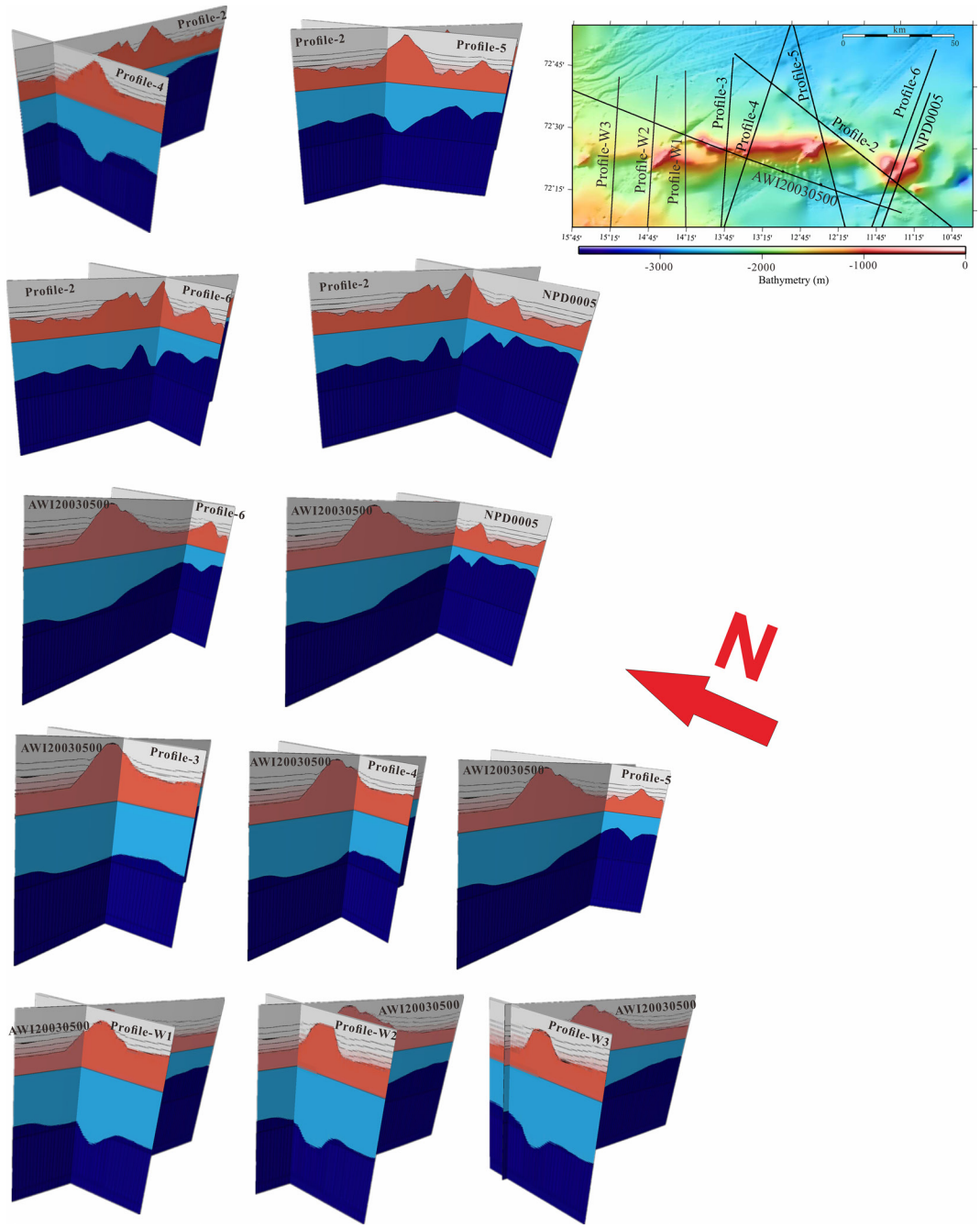

Figure 11. The ties between all the profiles. See the bathymetric map for locations. The upper two rows show the crustal structure correlation of Profile-2 with Profiles 4–6 and NPD0005. The lower three rows show the crustal structure correlation between the crustal model of AWI20030500 (Voss & Jokat, 2007) with Profiles 3–6, NPD0005, and Profiles-W1-3.

summit (20 vs. 10 km) as the Logi Ridge summit at its widest. They were both formed on young oceanic lithosphere, the Logi Ridge at around 5 Ma, and the northern LSC at around 10 Ma old lithosphere. However, the Louisville Guyot has velocity up to 7.5 km/s at the base of the crust, while velocities reach only 7 km/s at the Logi Ridge, and also lower crustal thickness is twice as large as that of the Logi Ridge (Figures 15a and 15b).

This difference in lower crustal velocity between the ridges indicates differences in the melting conditions. Since they both formed on young lithosphere, the melting is not confined to be deep only, and velocities can reflect temperature conditions primarily. If seismic velocity is plotted against crustal thickness (H-Vp analysis),

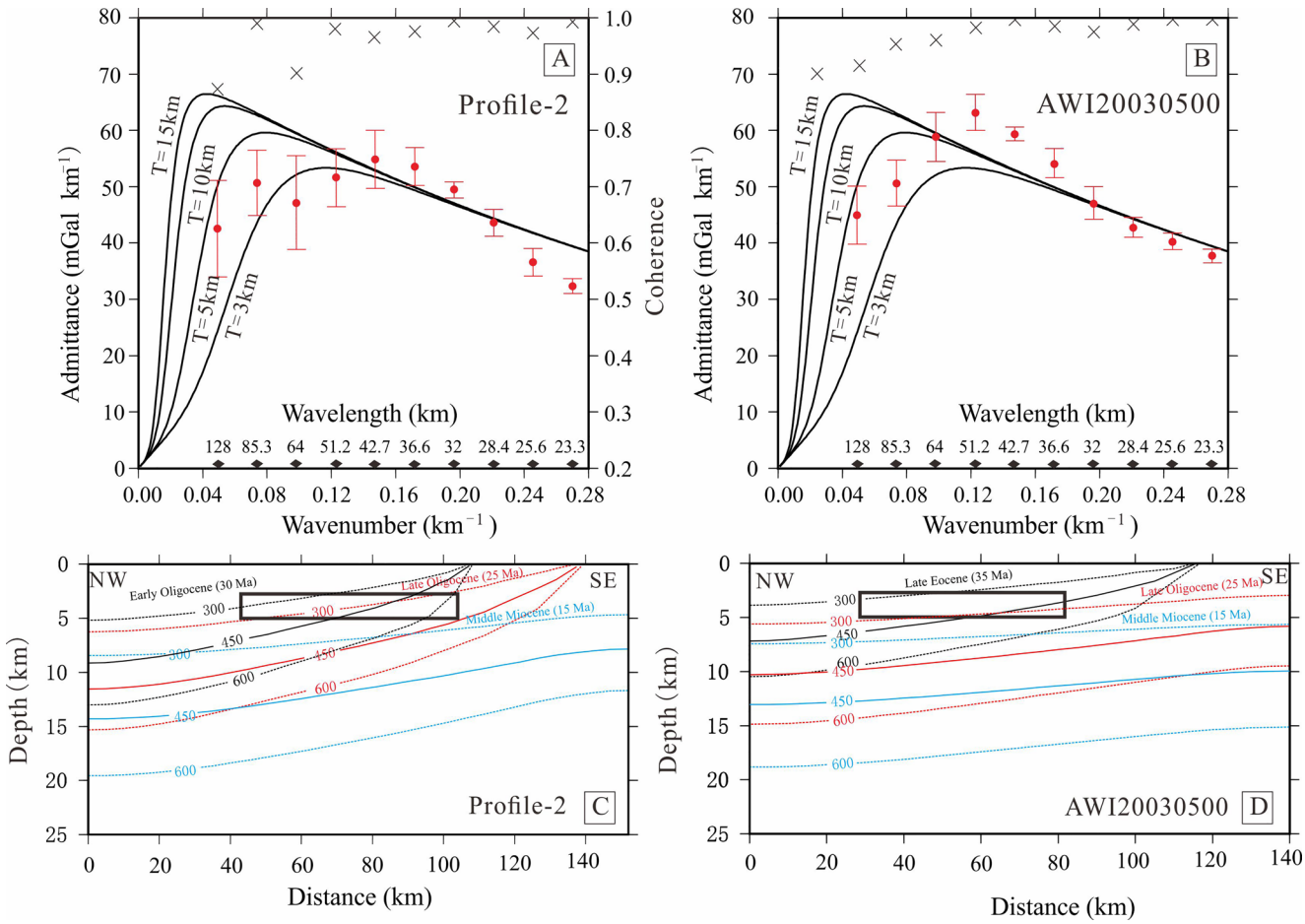

Figure 12. (a and b): The spectral admittance function between gravity and bathymetry (with 1 σ error bars) along Profile-2 and AWI20030500. Theoretical functions of different elastic plate thicknesses from 3 to 15 km are shown for comparison. The coherence is shown by crosses. (c and d): The modeled 450 ± 150° isotherm along the profiles from Early Oligocene (30–35 Ma) to Late Oligocene (25 Ma), to Middle Miocene (15 Ma) along Profile-2 and AWI20030500. The black box indicates the area of the Logi Ridge with an elastic thickness of 3–5 km covered by each profile.

the differences are quite apparent (Figure 15). With melting under the elevated mantle temperature, the melts produced will be rich in MgO content relative the FeO content (e.g., Sallarès et al., 2005; White, 1989), resulting in a positive correlation between the crustal thickness and seismic velocity (Holbrook et al., 2001). Part of the Logi Ridge crust was first created by melting at the spreading ridge and then by later melting building the ridge on the existing oceanic crust (Tan et al., 2019). If the Logi Ridge formation itself was mainly driven by the elevated mantle temperature, it should still result in a positive H-V_p correlation. However, there is a low H-Vp correlation for the Logi Ridge, where the Vp remains almost constant over crustal thickness variations from 5.5 to 11.5 km, which does not indicate elevated mantle temperature for the melting event (Figure 15). For the Louisville Guyot, there is a positive H-Vp correlation consistent with the elevated mantle temperature melting and its mantle plume origin. This comparison indicates that hot mantle melting should be visible, since both ridges otherwise were formed under similar settings.

There is a general trade-off between lower crustal velocity and Moho depth in velocity modeling, where the travel time delay of a deeper Moho can to some extent be reduced by increased lower crustal velocity. Voss and Jokat (2007) indicate a ±2 km Moho depth uncertainty coupled to a ±0.2 km/s lower crustal uncertainty for the model as a whole. We test it by increasing velocity and depth by this amount underneath the summit of the ridge in the AWI20030500 (Figure 15d). That results in a weakly positive H-Vp correlation, but still lower than that found at the northern Eggvin Bank for a seamount apparently formed off-ridge (Figure 15d) (Tan et al., 2017). It is therefore not possible to completely rule out that the elevated temperature contributes to the mantle melting though it seems unlikely that mantle melting was anywhere near as hot as it was for the Louisville Guyot.

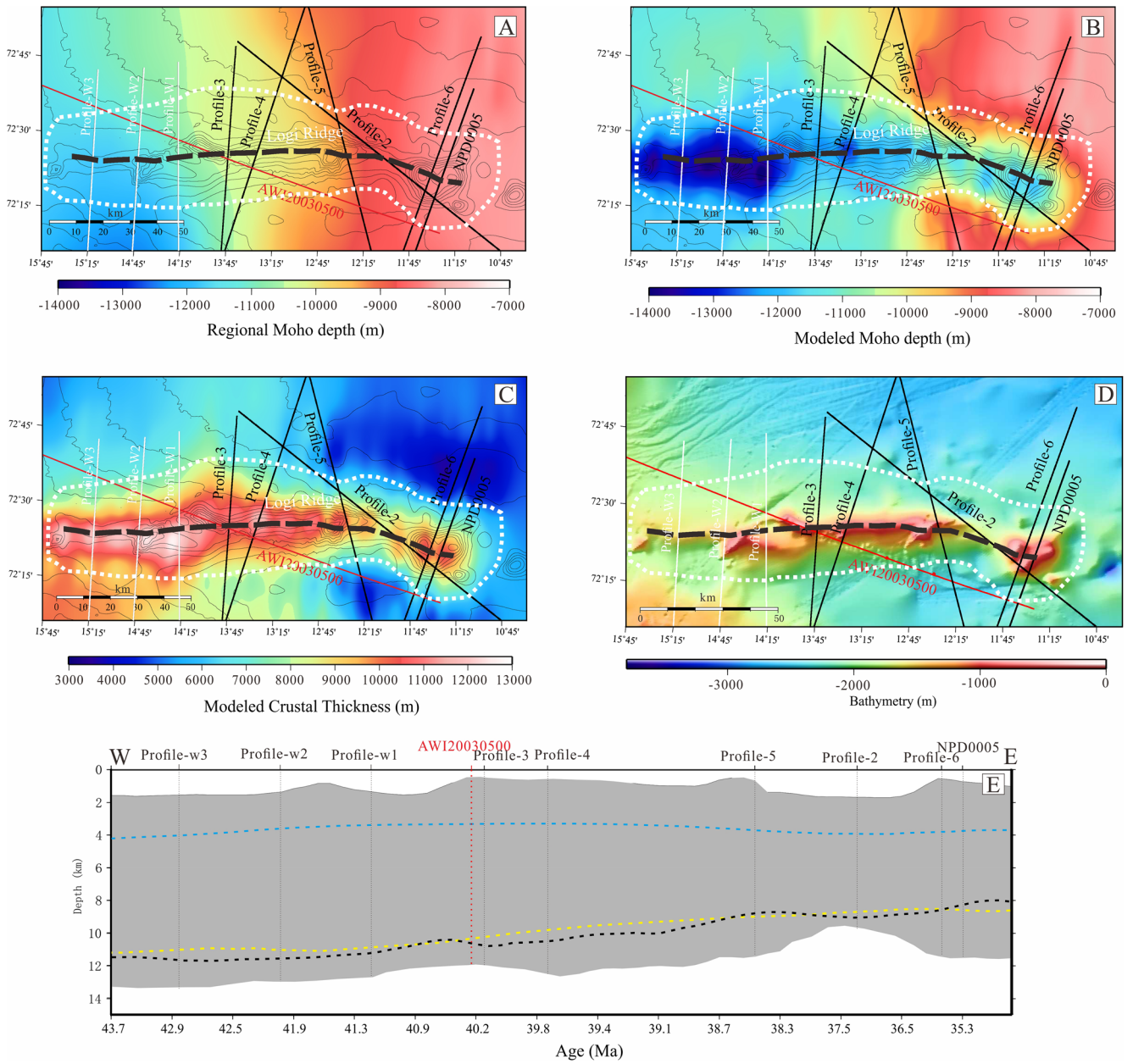

Figure 13. Modeled regional Moho depth (a), modeled Moho depth (b), modeled crustal thickness (c), and bathymetry map (d) of the study area. Thin black lines (a–c) show bathymetry contours at 250 m interval (Jakobsson et al., 2020). The extent of the Logi Ridge for volume calculations is indicated by the white-dotted line. (e): Crustal structure along the Logi Ridge derived along the thick dashed black line in Figures 13a–13d. The regional top basement (blue-dashed line) and the regional Moho depth (black-dashed line) are derived from our models. The yellow-dashed line is the regional Moho from Funck et al. (2016). The oceanic seafloor ages (Gaina et al., 2016) are indicated at the bottom. Ties with the models are indicated by dotted lines on the crustal transect.

As pointed out by Tan et al. (2019), the Logi Ridge is surrounded by an elevated platform, and Breivik et al. (2009) showed that the seafloor is ~1,200 m shallower there than that at the conjugate seafloor off the Norwegian coast. This corresponds to an area of dynamic topography (1–2 km) as shown by Rickers et al. (2013). Tan et al. (2019) demonstrated that this dynamic topography was developed coeval with the Logi Ridge development. It is expected to be caused by the outflow of material from the Iceland Plume with the extra buoyancy tied to elevated temperature (Parnell-Turner et al., 2014). Recent mantle tomography models show to a varying degree that there is reduced Vs velocity in the asthenosphere under the region of dynamic topography (Celli et al., 2021; Rickers et al., 2013), mostly on the western side of the spreading ridge. We also note that the Vesteris Seamount,

Table 1
Estimated Ridge-Area Magmatic Volumes and Production Rates With Uncertainties

	Area
Logi Ridge area	6.14×10^9 m^2
	Magmatic volume
Volume before Logi Ridge building	3.9×10^{13} m^3
Volume after Logi Ridge building	5.6×10^{13} m^3
Moho depth uncertainty ±1 km effect on volume	$\pm 0.6 \times 10^{13}$ m^3
Volume of the Logi Ridge with uncertainty	$(1.7 \pm 0.6) \times 10^{13}$ m^3
	Magmatic production rate
Minimum estimate (20 Ma duration)	$(0.02–0.04) \times 10^3$ m^3
Preferred estimate (5 Ma duration)	$(0.07–0.15) \times 10^3$ m^3

which has had recent volcanism (Haase & Devey, 1994), is located at the edge of this area of pronounced dynamic topography (Figure 1), though both the cited tomography models show a negative Vs anomaly underneath.

The Iceland plume is known to be geochemically heterogeneous, and geochemical results from nearby lend some support to the velocity model results. The northern segment of the Kolbensiey Ridge (Eggvin Bank) basalts just south of the Logi Ridge has a similar enriched isostopical composition as that of those from the southeastern volcanic zone (e.g., Vestmannaeyjar) and on the Reykjanes Peninsula in Iceland (e.g., Debaille et al., 2009; Mertz et al., 2004). This suggests that the Eggvin Bank was formed by a deeper asthenospheric flow of an enriched Iceland plume component entrained in the outer region of the plume (Mertz et al., 2004), which may also have affected the Logi Ridge formation. Such an enriched component may also have been present for the first 3 Ma after crustal breakup at the Vøring Plateau in combination with the elevated mantle temperature (Breivik et al., 2009, 2014). This is not seen farther south on the Møre-Faeroes margins (Breivik et al., 2006; White et al., 2008), nor on the conjugate JMMC margin (Breivik et al., 2012).

As the discussion above indicates, there is evidence of both enriched mantle as well as elevated mantle temperature in the region. The elevated temperature is not needed for the Vesteris Seamount to the north of the Logi Ridge (Haase & Devey, 1994), nor for the present magmatism at the spreading ridge of the Eggvin Bank to the south (Mertz et al., 2004). Furthermore, moderate temperature increase is indicated for one seamount on the off-ridge part of the Eggvin Bank (Tan et al., 2017), while another neighboring seamount is similar to the Logi Ridge in showing little indication of the elevated temperature (Figure 15). It seems probable that the enriched mantle component plays a role in the magmatism but likely with a minor elevation of the mantle temperature contributing to it. This has some similarity to the Cocos Ridge created by the Galapagos Hotspot, which does not have an obvious high-temperature signature (Sallarès et al., 2003). It could be more of a compositional plume than a very hot plume (Figure 14).

6. Summary and Conclusions

We use crustal velocity structure, magma volume, and magma production rates to determine the formation mechanism of the Logi Ridge. The crustal thickness underneath the Logi Ridge crest varies between approximately 10 and 12 km. The magma volume of the ridge is estimated to be $(1.7\pm 0.6) \times 10^{13} m^3$. The admittance analysis indicates an elastic plate thickness of 3–5 km at the time of the Logi Ridge emplacement, consistent with the ridge being formed on oceanic crust only a few million years old. Therefore, a construction time for the main part of the ridge of 5 Ma during the Oligocene seems reasonable, which gives a magma production rate of 0.07–0.15 m^3/s. That is comparable to the estimates for the LSC.

The Logi Ridge and the Louisville Guyot in the LSC are both formed on young oceanic lithosphere less than 10 Ma old. The Louisville Guyot shows a positive correlation between total crustal thickness and lower crustal velocity, showing that the elevated mantle temperature drove the mantle melting. The refraction profile across the Logi Ridge differs in that it does not show any high-velocity material in the lower crust, indicating that the melting was not caused by the significantly elevated mantle temperature. However, some temperature increase in the

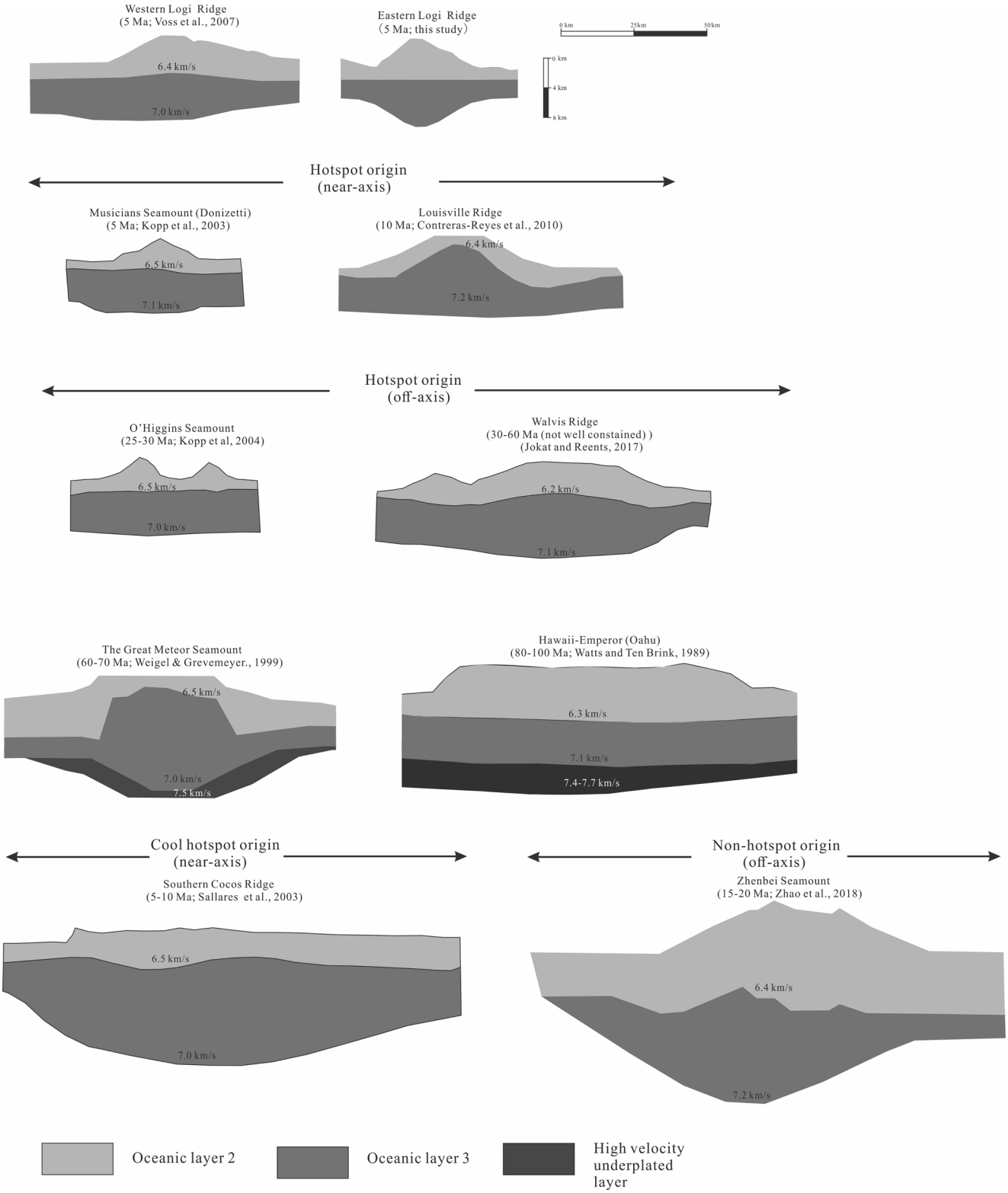

Figure 14.

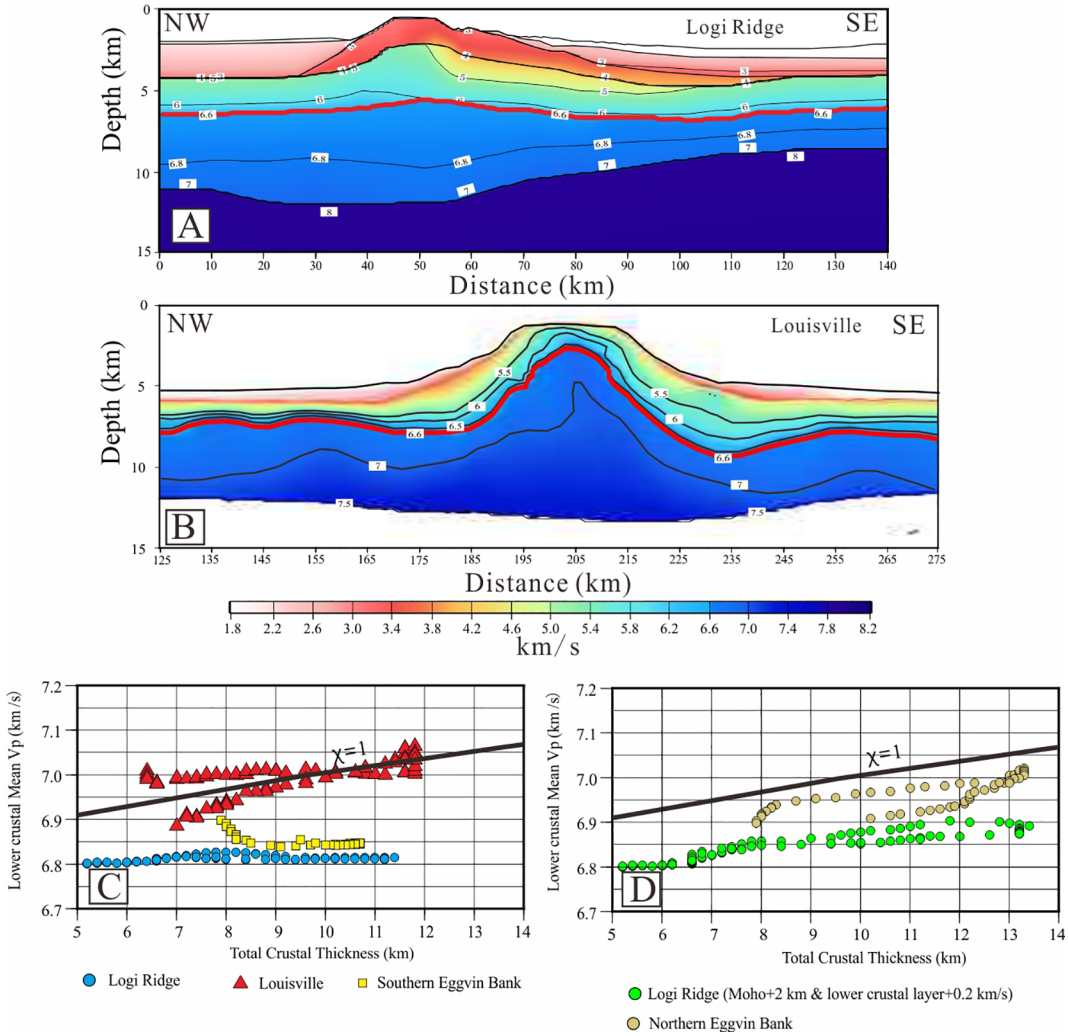

Figure 15. (a): The crustal velocity structure of the Logi Ridge (Voss & Jokat, 2007); (b): Intraplate seamount formed by the Louisville hot spot (Contreras-Reyes et al., 2010). The solid red line shows the boundary of the upper and lower crust on panels A and B. (c): Total crustal thickness versus average lower crustal velocity for the Logi Ridge from profile AWI20030500 and from the Louisville hot spot-induced seamount (Contreras-Reyes et al., 2010). The results from the seamount on the southern Eggvin Bank (Tan et al., 2017) is quite close to that of the model from the Logi Ridge. (d): Total crustal thickness versus average lower crustal velocity for the off-ridge northern Eggvin Bank (Tan et al., 2017) compared to the Logi Ridge maximum error model with 2 km deeper Moho and 0.2 km/s higher lower crustal velocity under the central part of the ridge from profile AWI20030500. For panels C and D, sampling interval is 2 km horizontally and the seismic velocity is pressure and temperature corrected (Holbrook et al., 2001). Magma productivity from passive decompression melting of mantle with increasing temperature is indicated by $\chi = 1$ (McKenzie & Bickle, 1988).

mantle is possible within the cited refraction model uncertainty. The ridge area has an elevated dynamic topography, which developed coeval with the ridge, and negative *Vs* anomalies are currently present in the mantle underneath, both indicating the elevated mantle temperature. On the other hand, melting at the adjacent Eggvin Bank on the northernmost Kolbeinsey spreading ridge segment to the south is derived from an enriched component

Figure 14. Logi Ridge crustal structure compared with on-axis and off-axis seamounts with hotspot and non-hotspot origins. The approximate age of the oceanic crust during the main formation of the seamount is also indicated. The western Logi Ridge is from seismic refraction data (Voss & Jokat, 2007), while the eastern Logi Ridge is from the 2D modeling in this study. Examples from Musicians seamount (Donizetti) (Kopp et al., 2003) and Louisville Ridge (Contreras-Reyes et al., 2010) show typical crustal structure of hot plume-induced seamount formed on young lithosphere, while the O'Higgins Seamount (Kopp et al., 2004), Walvis Ridge (Jokat & Reents, 2017), Great Meteor Seamount (Weigel & Grevemeyer, 1999), and Oahu Island (Hawii-Emperor chain) (Watts & Ten Brink, 1989) show the crustal structure of intraplate seamounts affected by a mantle plume on old oceanic lithosphere. Southern Cocos Ridge (Sallarès et al., 2003) and Zhenbei Seamount (Zhao et al., 2018) represent typical crustal structures of near-axis and off-axis seamounts without the signature of elevated temperature. A very high velocity underplated layer is only observed under intraplate seamounts affected by a hot plume with thick lithosphere. The plotting scale is shown on the top right corner of the figure.

present at the outer parts of the Iceland Plume, where the elevated temperature plays a lesser role. It therefore seems reasonable to conclude that an enriched mantle component contributes to the formation of the Logi Ridge, but probably combined with a moderate temperature increase in the mantle. There appears to be a complex interaction between mantle temperature and mantle heterogeneity that drives magmatism in the NE Atlantic. This is an important issue that needs further study through both geophysical and geochemical surveying in order to understand the dynamics of the Iceland Plume since crustal breakup and up to present.

Data Availability Statement

The data for this paper (e.g., crustal and lithospheric density model, 2D gravity modeling, and isostatic balancing) are available via the website https://figshare.com/s/106044fb069c1d3bf480.

Acknowledgments
We thank Wilfried Jokat and Graeme Eagles from Alfred Wegener Institute (AWI) for the seismic refraction model and ship-track free-air gravity of line AWI20030500. We also thank Eduardo Contreras-Reyes for the velocity model of the Louisville Guyot, and the reviewers Wifried Jokat, one anonymous, and associated editor for the many improvements they brought to the paper. This study is supported by Scientific Research Fund of the Second Institute of Oceanography, MNR, Grant Nos. HYGG2001, the Natural Science Foundation of China (42006072), Innovation Group Project of Southern Marine Science and Engineering Guangdong Laboratory (Zhuhai) (No.311020018), Qianjiang talent QJD2002033, and the Research Council of Norway through its Centers of Excellence funding scheme (project number 223272).

References

Abdelmalak, M. M., Planke, S., Faleide, J. I., Jerram, D. A., Zastrozhnov, D., Eide, S., & Myklebust, R. (2016). The development of volcanic sequences at rifted margins: New insights from the structure and morphology of the Vøring Escarpment, mid-Norwegian Margin. *Journal of Geophysical Research: Solid Earth*, *121*(7), 5212–5236. https://doi.org/10.1002/2015jb012788

Bai, Y., Williams, S. E., Müller, R. D., Liu, Z., & Hosseinpour, M. (2014). Mapping crustal thickness using marine gravity data: Methods and uncertainties. *Geophysics*, *79*(2), G27–G36. https://doi.org/10.1190/geo2013-0270.1

Blischke, A., Gaina, C., Hopper, J. R., Péron-Pinvidic, G., Brandsdóttir, B., Guarnieri, P., et al. (2017). The Jan Mayen microcontinent: An update of its architecture, structural development and role during the transition from the Ægir Ridge to the mid-oceanic Kolbeinsey Ridge. In *The NE Atlantic region A reappraisal of crustal structure, tectonostratigraphy and magmatic evolution*, Geological Society London, Special Publication, 447. https://doi.org/10.1144/SP447.5

Blischke, A., Stoker, M. S., Brandsdóttir, B., Hopper, J. R., Peron-Pinvidic, G., Ólavsdóttir, J., & Japsen, P. (2019). The Jan Mayen microcontinent's Cenozoic stratigraphic succession and structural evolution within the NE-Atlantic. *Marine and Petroleum Geology*, *103*, 702–737. https://doi.org/10.1016/j.marpetgeo.2019.02.008

Breivik, A., Mjelde, R., Faleide, J. I., Flueh, E., & Murai, Y. (2014). Magmatic development of the outer Vøring margin from seismic data. *Journal of Geophysical Research*, *119*, 6733–6755. https://doi.org/10.1002/2014JB011040

Breivik, A. J., Faleide, J. I., Mjelde, R., & Flueh, R. (2009). Magma productivity and early seafloor spreading rate correlation on the northern Vøring Margin, Norway – constraints on mantle melting. *Tectonophysics*, *468*, 206–223. https://doi.org/10.1016/j.tecto.2008.09.020

Breivik, A. J., Mjelde, R., Faleide, J. I., & Murai, Y. (2006). Rates of continental breakup magmatism and seafloor spreading in the Norway Basin – Iceland plume interaction. *Journal of Geophysical Research*, *111*(B07102). https://doi.org/10.1029/2005JB004004

Breivik, A. J., Mjelde, R., Faleide, J. I., & Murai, Y. (2012). The eastern Jan Mayen microcontinent volcanic margin. *Geophysical Journal International*, *188*, 798–818. https://doi.org/10.1111/j.1365-246x.2011.05307.x

Breivik, A. J., Verhoef, J., & Faleide, J. I. (1999). Effect of thermal contrasts on gravity modeling at passive margins: Results from the western Barents Sea. *Journal of Geophysical Research*, *104*(B7), 15293–15311. https://doi.org/10.1029/1998jb900022

Celli, N. L., Lebedev, S., Schaeffer, A. J., & Gaina, C. (2021). The tilted Iceland Plume and its effect on the North Atlantic evolution and magmatism. *Earth and Planetary Science Letters*, *569*, 117048. https://doi.org/10.1016/j.epsl.2021.117048

Contreras-Reyes, E., Grevemeyer, I., Watts, A., Planert, L., Flueh, E. R., & Peirce, C. (2010). Crustal intrusion beneath the Louisville hotspot track. *Earth and Planetary Science Letters*, *289*(3–4), 323–333. https://doi.org/10.1016/j.epsl.2009.11.020

Debaille, V., Trønnes, R. G., Brandon, A. D., Waight, T. E., Graham, D. W., & Lee, C. A. (2009). Primitive off-rift basalts from Iceland and Jan Mayen: Os-isotopic evidence for a mantle source containing enriched subcontinental lithosphere. *Geochimica et Cosmochimica Acta*, *73*, 3423–3449. https://doi.org/10.1016/j.gca.2009.03.002

Elkins, L. J., Hamelin, C., Blichert-Toft, J., Scott, S. R., Sims, K. W. W., Yeo, I. A., et al. (2016). North Atlantic hotspot-ridge interaction near Jan Mayen Island. *Geochem. Persp. Lett.*, *2*, 55–67. https://doi.org/10.7185/geochemlet.1606

Elkins, L. J., Sims, K. W. W., Prytulak, J., Elliott, T., Mattielli, N., Blichert-Toft, J., et al. (2011). Understanding melt generation beneath the slow-spreading Kolbeinsey Ridge using ^{238}U, ^{230}Th, and ^{231}Pa excesses. *Geochimica et Cosmochimica Acta*, *75*, 6300–6329. https://doi.org/10.1016/j.gca.2011.08.020

Engen, Ø., Frazer, L. N., Wessel, P., & Faleide, J. I. (2006). Prediction of sediment thickness in the Norwegian–Greenland Sea from gravity inversion. *Journal of Geophysical Research: Solid Earth*, *111*, B11403. https://doi.org/10.1029/2005JB003924

Franke, D., Klitzke, P., Barckhausen, U., Berglar, K., Berndt, C., Damm, V., et al. (2019). Polyphase magmatism during the formation of the northern East Greenland continental margin. *Tectonics*, *38*, 2961–2982. https://doi.org/10.1029/2019tc005552

Funck, T., Geissler, W. H., Kimbell, G. S., Gradmann, S., Erlendsson, Ö., McDermott, K., & Petersen, U. K. (2016). Moho and basement depth in the NE Atlantic Ocean based on seismic refraction data and receiver functions. *Geological Society - Special Publications*, *477*. https://doi.org/10.1144/SP447.1

Gaina, C., Blischke, A., Geissler, W. H., Kimbell, G. S., & Erlendsson, Ö. (2016). Seamounts and oceanic igneous features in the NE Atlantic: A link between plate motions and mantle dynamics. *Geological Social London Special Publications*, *447*(1), 419–442. https://doi.org/10.1144/sp447.6

Gaina, C., Nasuti, A., Kimbell, G. S., & Blischke, A. (2017). Break-up and seafloor spreading domains in the NE Atlantic. *Geological Social London Special Publications*, *447*, 393–417. https://doi.org/10.1144/sp447.12

Gaina, C., Werner, S. C., Saltus, R., Maus, S., & GROUP, T. C.-G. (2011). Circum-Arctic mapping project: New magnetic and gravity anomaly maps of the Arctic. *Journal of the Geological Society*, *35*, 39–48. https://doi.org/10.1144/m35.3

Geissler, W. H., Gaina, C., Hopper, J. R., Funck, T., Blischke, A., Arting, U., et al. (2017). Seismic volcanostratigraphy of the NE Greenland continental margin. *Geological Social London Special Publications*, *447*(1), 149–170. https://doi.org/10.1144/sp447.11

Haase, K. M., & Devey, C. W. (1994). The petrology and geochemistry of Vesteris Seamount, Greenland Basin – An intraplate alkaline volcano of non-plume origin. *Journal of Petrology*, *35*(2), 295–328. https://doi.org/10.1093/petrology/35.2.295

Haase, K. M., Devey, C. W., & Wieneke, M. (2003). Magmatic processes and mantle heterogeneity beneath the slow-spreading northern Kolbeinsey Ridge segment, North Atlantic. *Contributions to Mineralogy and Petrology*, *144*, 428–448. https://doi.org/10.1007/s00410-002-0408-z

Hermann, T., & Jokat, W. (2016). Crustal structure off Kong Oscar Fjord, east Greenland: Evidence for focused melt supply along the Jan Mayen fracture zone. *Tectonophysics*, *691*, 110–119. https://doi.org/10.1016/j.tecto.2015.12.005

Holbrook, W. S., Larsen, H. C., Korenaga, J., Dahl-Jensen, T., Reid, I. D., Kelemen, P. B., et al. (2001). Mantle thermal structure and active upwelling during continental breakup in the North Atlantic. *Earth and Planetary Science Letters*, *190*, 251–266. https://doi.org/10.1016/s0012-821x(01)00392-2

Jakobsson, M., Mayer, L., Bringensparr, C., Castro, C. F., Mohammad, R., Johnson, P., et al. (2020). The international bathymetric chart of the Arctic ocean version 4.0. *Scientific Data*, *7*, 176. https://doi.org/10.1038/s41597-020-0520-9

Jokat, W., & Reents, S. (2017). Hotspot volcanism in the southern south Atlantic: Geophysical constraints on the evolution of the southern Walvis Ridge and the discovery seamounts. *Tectonophysics*, *716*, 77–89. https://doi.org/10.1016/j.tecto.2016.12.011

Kandilarov, A., Mjelde, R., Pedersen, R. B., Hellevang, B., Papenberg, C., Petersen, C. J., et al. (2012). The northern boundary of the Jan Mayen Microcontinent, North Atlantic determined from ocean bottom seismic, multichannel seismic, and gravity data. *Marine Geophysical Researches*, *33*(1), 55–76. https://doi.org/10.1007/s11001-012-9146-4

Kodaira, S., Mjelde, R., Gunnarsson, K., Shiobara, H., & Shimamura, H. (1998a). Evolution of oceanic crust on the Kolbeinsey Ridge, north of Iceland, over the past 22 Myr. *Terra Nova*, *10*, 27–31. https://doi.org/10.1046/j.1365-3121.1998.00166.x

Kodaira, S., Mjelde, R., Gunnarsson, K., Shiobara, H., & Shimamura, H. (1998b). Structure of the Jan Mayen microcontinent and implication for its evolution. *Geophysical Journal International*, *132*, 383–400. https://doi.org/10.1046/j.1365-246x.1998.00444.x

Kopp, H., Flueh, E. R., Papenberg, C., & Klaeschen, D. (2004). Seismic investigations of the O'Higgins seamount Group and Juan Fernández Ridge: Aseismic Ridge emplacement and lithosphere hydration. *Tectonics*, *23*, TC2009. https://doi.org/10.1029/2003TC001590

Kopp, H., Kopp, C., Morgan, J. P., Flueh, E. R., Weinrebe, W., & Morgan, W. J. (2003). Fossil hot spot-ridge interaction in the Musicians Seamount Province: Geophysical investigations of hot spot volcanism at volcanic elongated ridges. *Journal of Geophysical Research*, *108*(B3), 2160. https://doi.org/10.1029/2002JB002015

Koppers, A. A., & Watts, A. B. (2010). Intraplate seamounts as a window into deep Earth processes. *Oceanography*, *23*(1), 42–57. https://doi.org/10.5670/oceanog.2010.61

Larsen, L. M., Pedersen, A. K., Tegner, C., & Duncan, R. A. (2014). Eocene to Miocene igneous activity in NE Greenland: Northward younging of magmatism along the east Greenland margin. *Journal of the Geological Society*, *171*(4), 539–553. https://doi.org/10.1144/jgs2013-118

Lee, T.-C., Rudman, A., & Sjoreen, A. (1980). *Application of finite element analysis to terrestrial heatflow, Occas. Pap*, (Vol. 20, p. 53), Deptment of Natural Resources, Geological Survey.

Lonsdale, P. (1988). Geography and history of the Louisville hotspot chain in the southwest Pacific. *Journal of Geophysical Research*, *93*, 3078–3104. https://doi.org/10.1029/jb093ib04p03078

McKenzie, D., & Bickle, M. J. (1988). The volume and composition of melt generated by extension of the lithosphere. *Journal of Petrology*, *29*(3), 625–679. https://doi.org/10.1093/petrology/29.3.625

Mertz, D. F., Sharp, W. D., & Haase, K. M. (2004). Volcanism on the Eggvin Bank (central Norwegian-Greenland sea, latitude ~71°N): Age, source, and relationship to the Iceland and putative Jan Mayen plumes. *Journal of Geodynamics*, *38*, 57–83. https://doi.org/10.1016/j.jog.2004.03.003

Mjelde, R., Breivik, A. J., Raum, T., Mittelstaedt, E., Ito, G., & Faleide, J. I. (2008). Magmatic and tectonic evolution of the north Atlantic. *Journal of the Geological Society*, *165*, 31–42. https://doi.org/10.1144/0016-76492007-018

Mjelde, R., & Faleide, J. (2009). Variation of Icelandic and Hawaiian magmatism: Evidence for co-pulsation of mantle plumes? *Marine Geophysical Researches*, *30*(1), 61–72. https://doi.org/10.1007/s11001-009-9066-0

Mjelde, R., Wessel, P., & Müller, R. D. (2010). Global pulsations of intraplate magmatism through the Cenozoic. *Lithosphere*, *2*(5), 361–376. https://doi.org/10.1130/l107.1

National Geophysical Data Center. (2006). *2-minute gridded global relief data (ETOPO2) v2*. National Geophysical Data Center. https://doi.org/10.7289/V5J1012Q

Noble, R. H., Macintyre, R. M., & Brown, P. E. (1988). Age constraints on Atlantic evolution: Timing of magmatic activity along the E Greenland continental margin. *Geological Society - Special Publications*, *39*, 201–214. https://doi.org/10.1144/GSL.SP.1988.039.01.19

Nunns, A. (1982). The structure and evolution of the Jan Mayen Ridge and surrounding regions. In J. S. Watkins & C. L. Drake (Eds.), (Vol. 34, pp. 193–208). Am. Assoc. Petrol. Geol. https://doi.org/10.1306/m34430c10

Parnell-Turner, R., White, N., Henstock, T., Murton, B., Maclennan, J., & Jones, S. M. (2014). A continuous 55-million-year record of transient mantle plume activity beneath Iceland. *Nature Geoscience*, *7*(12), 914–919. https://doi.org/10.1038/ngeo2281

Price, S., Brodie, J., Whitham, A., & Kent, R. (1997). Mid-Tertiary rifting and magmatism in the Traill Ø region, East Greenland. *Journal of the Geological Society*, *154*, 419–434. https://doi.org/10.1144/gsjgs.154.3.0419

Richards, M., Contreras-Reyes, E., Lithgow-Bertelloni, C., Ghiorso, M., & Stixrude, L. (2013). Petrological interpretation of deep crustal intrusive bodies beneath oceanic hotspot provinces. *Geochemistry, Geophysics, Geosystems*, *14*(3), 604–619. https://doi.org/10.1029/2012gc004448

Rickers, F., Fichtner, A., & Trampert, J. (2013). The Iceland-Jan Mayen plume system and its impact on mantle dynamics in the North Atlantic region: Evidence from full-waveform inversion. *Earth and Planetary Science Letters*, *367*, 39–51. https://doi.org/10.1016/j.epsl.2013.02.022

Sallarès, V., & Calahorrano, A. (2007). Geophysical characterization of mantle melting anomalies: A crustal view. *Geological Society Special Paper*, *430*, 507–524. https://doi.org/10.1130/2007.2430(25)

Sallarès, V., Charvis, P., Flueh, E. R., & Bialas, J. (2003). Seismic structure of Cocos and Malpelo Volcanic Ridges and implications for hot spot-ridge interaction. *Journal of Geophysical Research*, *108*(B12), 2564. https://doi.org/10.1029/2003JB002431

Sallarès, V., Charvis, P., Flueh, E. R., Bialas, J., & the SALIERI Scientific Party. (2005). Seismic structure of the Carnegie ridge and the nature of the Galápagos hotspot. *Geophysical Journal International*, *161*, 763–788. https://doi.org/10.1111/j.1365-246X.2005.02592.x

Schilling, J. (1999). Dispersion of the Jan Mayen and Iceland mantle plumes in the Arctic: A He-Pb-Nd-Sr isotope tracer study of basalts from the Kolbeinsey, Mohns, and Knipovich Ridges. *Journal of Geophysical Research*, *104*, 10543–10569. https://doi.org/10.1029/1999jb900057

Talwani, M., Worzel, J. L., & Landisman, M. G. (1959). Rapid gravity computations for two-dimensional bodies with application to the Mendocino submarine fracture zone. *Journal of Geophysical Research*, *64*, 49–59. https://doi.org/10.1029/jz064i001p00049

Tan, P., Breivik, A. J., & Mjelde, R. (2019). Dynamic topography development north of Iceland from subaerial exposure of the igneous Logi Ridge, NE Atlantic. *Journal of Geophysical Research: Solid Earth*, *124*, 10799–10822. https://doi.org/10.1029/2019JB017603

Tan, P., Breivik, A. J., Trønnes, R. G., Mjelde, R., Azuma, R., & Eide, S. (2017). Crustal structure and origin of the Eggvin Bank west of Jan Mayen, NE Atlantic. *Journal of Geophysical Research: Solid Earth*, *122*, 43–62. https://doi.org/10.1002/2016JB013495

Tan, P., Sippel, J., Breivik, A. J., Meeßen, C., & Scheck-Wenderoth, M. (2018). Lithospheric control on asthenospheric flow from the Iceland plume: 3D density modeling of the Jan Mayen-East Greenland region, NE Atlantic. *Journal of Geophysical Research: Solid Earth*, *123*, 9223–9248. https://doi.org/10.1029/2018JB015634

Trønnes, R. G., Planke, S., Sundvoll, B., & Imsland, P. (1999). Recent volcanic rocks from Jan Mayen: Low-degree melt fractions of enriched northeast Atlantic mantle. *Journal of Geophysical Research*, *104*(B4), 7153–7168.

Van Ark, E. M., & Lin, J. (2004). Time variation in igneous volume flux of the Hawaii-Emperor hot spot seamount chain. *Journal of Geophysical Research*, *109*(B11), 401. https://doi.org/10.1029/2003jb002949

Verhoef, J., Roest, W. R., Macnab, R., Arkani-Hamed, J., et al. (1996). Magnetic anomalies of the Arctic and north Atlantic oceans and adjacent land areas, *Tech. rep*. Geol. Surv. Canada.

Voss, M., & Jokat, W. (2007). Continent-ocean transition and voluminous magmatic underplating derived from P-wave velocity of the East Greenland continental margin. *Geophysical Journal International*, *170*, 580–604. https://doi.org/10.1111/j.1365-246X.2007.03438.x

Voss, M., Schmidt-Aursch, M. C., & Jokat, W. (2009). Variations in magmatic processes along the East Greenland volcanic margin. *Geophysical Journal International*, *177*, 755–782. https://doi.org/10.1111/j.1365-246x.2009.04077.x

Watts, A. B. (1978). An analysis of isostasy in the world's oceans 1. Hawaiian–Emperor seamount chain. *Journal of Geophysical Research*, *83*(B12), 5989–6004. https://doi.org/10.1029/jb083ib12p05989

Watts, A. B., & Ten Brink, U. S. (1989). Crustal structure, flexure, and subsidence history of the Hawaiian Islands. *Journal of Geophysical Research*, *94*, 10473–10500. https://doi.org/10.1029/jb094ib08p10473

Weigel, W., & Grevemeyer, I. (1999). The Great Meteor seamount: Seismic structure of a submerged intraplate volcano. *Journal of Geodynamics*, *28*(1), 27–40. https://doi.org/10.1016/s0264-3707(98)00030-1

Wessel, P., & Smith, W. H. F. (1991). Free software helps map and display data. *Eos Trans. AGU*, *72*(441), 445–446. https://doi.org/10.1029/90eo00319

White, R. S. (1989). Initiation of the Iceland plume and opening of the north Atlantic. In A. J. Tankard & H. R. Balkwill (Eds.), *Extensional tectonics and stratigraphy of the North Atlantic margins*. AAPG mem. (Vol. 46, pp. 149–154). https://doi.org/10.1306/m46497c10

White, R. S., McKenzie, D., & O'Nions, K. (1992). Oceanic crustal thickness from seismic measurements and rare earth element inversion. *Journal of Geophysical Research*, *97*(B13), 19683–19715. https://doi.org/10.1029/92jb01749

White, R. S., Smith, L. K., Roberts, A. W., Christie, P. A. F., & Kusznir, N. J., & iSIMM Team. (2008). Lower-crustal intrusion on the North Atlantic continental margin. *Nature*, *452*, 460–464. https://doi.org/10.1038/nature06687

Zelt, C. A., & Smith, R. B. (1992). Seismic traveltime inversion for 2-D crustal velocity structure. *Geophysical Journal International*, *108*, 16–34. https://doi.org/10.1111/j.1365-246x.1992.tb00836.x

Zhao, M., He, E., Sibuet, J., Sun, L., Qiu, X., Tan, P., & Wang, J. (2018). Postseafloor spreading volcanism in the central east south China sea and its formation through an extremely thin oceanic crust. *Geochem.Geophys.Geosyst.*, *19*(3), 621–641. https://doi.org/10.1002/2017gc007034